NPG Asia Materials (2013) 5, e43; doi:10.1038/am.2012.73

www.nature.com/am

REVIEW

Nanoscale assembly into extended and continuous structures and hybrid materials

Todd Emrick and Emily Pentzer

Harnessing synthetic power to create novel materials with unique assembly properties is of fundamental interest for pushing the limits of molecular and macromolecular assembly, while further holding the potential for improving electronic and medical device performance. Controlling the assembly of aromatic molecules into nanostructures provides routes towards continuous and extended structures with performance that is improved markedly over that of their individual molecular components, opening possibilities for the formation of composites that have tailored interactions with other materials and thus improved applications. This review covers recent advances in the synthesis of conjugated materials, their controlled assembly into nanoscale architectures and implementation into devices. Specifically, we discuss the solution-based assembly of polythiophene into nanowire fibrils, the formation of columnar stacks of hexabenzocoronene liquid crystals and the preparation of functionalized solution processible graphene for nanocomposite formation.
NPG Asia Materials (2013) **5,** e43; doi:10.1038/am.2012.73; published online 22 March 2013

Keywords: graphene; hexabenzocoronene; nanocomposite; organic semiconductors; polymer; polythiophene; solution assembly

INTRODUCTION

The transformation of polymer materials from conventional engineering plastics to structures that form key components of electronic and medical devices is underpinned by the rapid pace of discovery and development of nanoscale structures having exquisite properties. The further manipulation of nanoscale materials into hybrid and hierarchical structures generates macroscopic materials that span multiple length scales, and that are ideal for combining optimal electronic and mechanical properties into one material or device configuration. Although polymer materials alone are desirable for enabling many technological processes (for example, conventional photolithography and flash memory), the past 10+ years have seen the development of numerous advances in hybrid materials involving nanoscale 'additives'. Such additives can be divided into two broad classes: (1) discrete metallic, semiconductor, and insulating particles having any of a variety of shapes and (2) all carbon-based π-conjugated 2D structures that include discrete objects such as fullerenes, or extended structures such as carbon nanotubes and graphene sheets.

This review considers the parallel development of nanostructured polymeric and all carbon materials, with particular emphasis on: (1) controlling the solution interactions of synthetic polymers, especially conjugated polymers, to produce robust objects that span multiple length scales as wires, sheets or ribbons, and that can further hybridize in a controllable manner with added nanoparticles (Section I), and (2) the structural evolution in the chemistry and assembly of all carbon materials, ranging from fused aromatic structures such as coronene, graphene and their functionalized derivatives (Section II). All of these materials are candidates for integration into functional devices, including solar cells, which in principle benefit from charge transport through the extended, continuous or network structures that form.

The structures we describe, and their associated applications, evolved from advances in numerous fields, including (1) clever and scalable synthetic chemistry for the preparation of polymers having well-defined backbone structure and architecture found for example, in Grignard metathesis polymerization for the preparation of regioregular poly(alkyl thiophenes); (2) interfacial and physical chemistry associated with the precise assembly of polymers and hybrid materials in solution and on surfaces, such as in the formation of nanowire fibrils from conjugated polymers; and (3) device design and evaluation that seeks to connect synthetic and physical advances with state-of-the-art performance in polymer and hybrid materials devices such as solar cells.

POLY(ALKYL THIOPHENE)-BASED MATERIALS AND ASSEMBLIES

Synthetic methods and solution-driven assemblies

Among synthetic polymers recognized for their optoelectronic properties, poly(3-hexyl thiophene) (P3HT) is established as both exceptionally popular and useful for organic/polymer electronics and photovoltaics (PVs).[1] The intrinsic hole carrying properties of P3HT, and its relatively simple synthesis, combine to broaden its appeal and availability. In P3HT (Figure 1a), covalently connected thiophenes comprise the conjugated polymer backbone and provide

Polymer Science and Engineering Department, University of Massachusetts Amherst, Amherst, MA, USA
Correspondence: Professor T Emrick, Polymer Science and Engineering Department, University of Massachusetts Amherst, 120 Governors Dr, Amherst, MA 01003, USA.
E-mail: tsemrick@mail.pse.umass.edu
Received 7 October 2012; revised 24 November 2012; accepted 3 December 2012

the desired electronic properties, while *n*-hexyl groups extend from the 3-position of each thiophene ring, giving solubility for controlled synthesis and processing. Polythiophene syntheses originated in electropolymerization,[2] later evolving to the now widely used metal catalyzed methodologies including Rieke metals,[3] and Grignard metathesis (GRIM) as pioneered by Yokozawa[4,5] and McCullough.[6,7] These synthetic advances have proven exceptionally useful for preparing P3HT and numerous functional polythiophene derivatives of controlled molecular weight (MW) and low MW distribution, both key features for understanding structure−property relationships. Building on these chemistries, researchers continue to advance polythiophene syntheses, seen for example, in the work of Kiriy[8] and Luscombe,[9,10] in which initiation/propagation kinetics are tuned by balancing steric and electronic interactions of aryl halide initiators and metal catalysts. Such advances enable efficient surface-initiated polymerization for covalent connection of P3HT to plastic, metallic and semiconductor substrates,[10,11] as well as the fabrication of star or branched macromolecular architectures from multifunctional initiators.[8,9,12]

The backbone conjugation of P3HT allows charge transport along the chain, while transport between polymer chains is provided by the interchain π-stacking in crystallized nanowires. P3HT fibril formation can occur in the solid state upon annealing, or under certain solvent conditions, such as the solution crystallization of the polymer on going from an initial 'good' solvent to a marginal or poor solvent environment[13] as described in early work of Smith[13] for polythiophene whiskers, and more recently in the elegant assembly and device structures of Jenekhe and Guillerez.[14,15] The resultant P3HT nanowires are composed of rigid, linear polymer chains held at an interchain spacing of 3.6 Å (determined by X-ray crystallography), typical of π-stacked systems. Transmission electron microscopy (TEM) of P3HT fibrils, obtained after drying, reveals striking images: impressively long continuous structures wind for hundreds of microns at a constant nanoscale width of ∼10–30 nm (Figure 1b).

UV–vis and photoluminescence (PL) spectroscopy mark the transformation of dissolved polymer to continuous fibril structures; in a good solvent such as chloroform the polymer is fully solvated, with absorption and PL maxima at ∼450 and 590 nm, respectively (Figure 1c). Introducing small amounts of a poor solvent such as dichloromethane or methanol promotes rapid interchain stacking, giving the wire-like fibrils (Figure 1b) as stably suspended structures. Fibril formation is accompanied by a red shift in absorption compared with solvated P3HT, and the formation of vibronic absorption maxima at 515, 550 and 605 nm (Figure 1c), correlating to excitation from the ground state to different vibronic excited states (that is, (0,2), (0,1) and (0,0) transitions, respectively).[16] A red shift in PL emission to 675 nm is observed, as well as a dramatic decline in PL emission intensity.

Individual P3HT fibrils can merge into collective assemblies by manipulating solvent strength and fibril concentration. P3HT fibrils can assemble into flat nanoribbons, many microns in length and, intriguingly, hundreds of nanometers in diameter suggesting a side-to-side arrangement of multiple individual fibrils.[17] These ribbon assemblies form only at low P3HT MW (below 10 kDa), implying that interfibril association is prevented by chain folding and hairpins at the fibril edges when using higher MW polymer. Certain solvents yield impressive branched structures composed of a column of ribbon-like P3HT with fibrils emanating normal to the long axis of the ribbon trunk, presumably due to a nucleated growth mechanism (Figure 1d).[18]

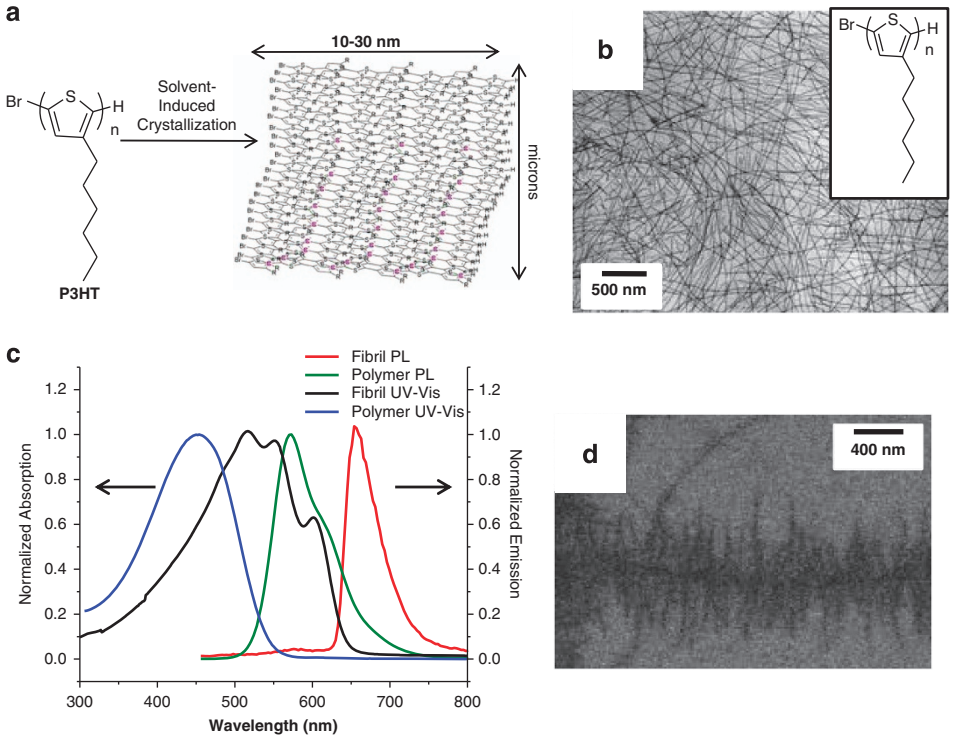

Figure 1 (**a**) Structure of regioregular poly(3-hexyl thiophene) (P3HT) and resultant fibrils induced by crystallization of the polymer backbone. (**b**) TEM image of P3HT fibrils formed by solvent-induced crystallization. Reprinted with permission from Wu *et al.*[19] Copyright 2009 American Chemical Society. (**c**) Normalized UV–vis (black) and PL (red, $\lambda_{exc} = 450$ nm) spectra of P3HT fibrils and UV–vis (blue) and PL (green, $\lambda_{exc} = 450$ nm) of solvated polymer. (**d**) P3HT fibrils emanating from a central ribbon-like core. Reprinted with permission from Yan *et al.*[18] Copyright 2011 American Chemical Society.

Electronic properties of polythiophene fibrils

The charge mobility of polythiophene fibrils as thin films can be characterized in field effect transistor (FET) measurements, performed parallel to the underlying substrate, and short circuit limited current (SCLC) measurements performed normal to the substrate (as for a solar cell). Fibril directionality can lead to different values from these two measurements, and control over fibril orientation can improve the FET- or SCLC-derived mobility values. However, fibrils are randomly oriented in thin films, and thus similar values are obtained for the two measurements. Hole mobility in thin films of free P3HT chains, cast from a 'good' solvent, are generally $10^{-5}-10^{-4}\,cm^2\,V^{-1}\,s^{-1}$;[20,21] increasing to $10^{-2}\,cm^2\,V^{-1}\,s^{-1}$ in annealed films, or films of preassembled fibrils cast from solution.[22] P3HT cast from higher boiling solvents (for example, chlorobenzene), or with high boiling additives (for example, diiodooctane), give mobility values close to those of solution-assembled fibrils, enabled by polymer crystallization during drying.[23,24] The mobility of poly (3-alkyl thiophene) fibrils varies little with choice of alkyl chain (C4 −C10), though mobility values for individual wires ($3-6\times10^{-2}\,cm^2\,V^{-1}\,s^{-1}$) are slightly higher than those of nanowire networks ($1-2\times10^{-2}\,cm^2\,V^{-1}\,s^{-1}$), attributed to a barrier to charge transport between fibrils within the thin films.[25]

The high hole mobility of P3HT nanowires is attractive for organic PVs, especially when combined with electron carriers, such as fullerenes. PV devices having active layers fabricated from solution-assembled poly(3-alkyl thiophene) nanowires display power conversion efficiency (PCE) values comparable with optimized devices that require annealing of P3HT/fullerene films;[15,19,26,27] for example, blending phenyl C_{61}−butyric acid methyl ester ($PC_{60}BM$) with P3HT fibrils gave devices with a 3.9% PCE, significantly higher than that obtained for thin films of noncrystallized P3HT and $PC_{60}BM$ (1.1%), and on par with annealed thin films (3.7%).[28] Active layers prepared by deposition of solution-prepared fibrils do not suffer from the vertical phase separation of the polymer and fullerene components, as observed during thermal annealing of conventional thin films.[29]

As PV device performance is influenced by a delicate balance of polymer crystallinity and active layer morphology, fibrils prepared in solution offer opportunities to enhance the understanding of structure−property relationships and improve device efficiency. When pure P3HT fibrils, isolated by centrifugation, were blended with solvated P3HT and $PC_{60}BM$ at various ratios, the highest PCE (3.6%) was obtained with ∼75% of the polymer in fibril form.[14] Advantageous coexistence of amorphous and crystalized (fibrilized) polymer was attributed to the presence of charge carrying bridges between fibril domains. Moreover, Lam reported solvent quality as a key parameter influencing device efficiency for P3HT nanowire/$PC_{60}BM$ devices—obtaining a 2.3% PCE when casting the active layer from 1:9 chlorobenzene:anisole, but only 1.4% when using pure chlorobenzene, and 2.1% with 1:4 chlorobenzene:anisole.[30] By fine-tuning the proportion of 'good' (chlorobenzene) and 'marginal' (anisole) solvents, the extent of polymer crystallinity (determined by UV–vis absorption and grazing incidence X-ray diffraction) was controlled, and device performance optimized.

Hybrid structures from solution assembly

PV devices with an active layer of polythiophene blended with electron carrying nanostructures, such as CdSe quantum dots (QDs) and nanorods (NRs), have been studied extensively,[31] yet only recently have P3HT nanowires have been examined in such devices. Greenham and co-workers[32] studied fibril formation during drying of the PV active layer in blends with pyridine-functionalized CdSe NRs, achieving a PCE of 2.6% at 90 wt% CdSe, an improvement over films of blended polymer and CdSe. In another approach, a solvent exchange technique was used by Wei and co-workers[33] to form hybrid structures of preformed P3HT fibrils that showed associated CdSe QDs by TEM, attributed to noncovalent interactions between the thiophene sulfur and QD surface. Subsequently, Gradečak and co-workers[34] used similar CdS−P3HT nanowire structures to produce efficient solar cells by minimizing macrophase segregation and maximizing domain interface (Figure 2a). Compared with a PCE of 0.6% for simple CdS/P3HT fibril blends, the solution-assembled structures produced an impressively high PCE of 4.1% at 80 wt% CdS, owing to better charge separation and enhanced charge collection.

Synthetic advances to give P3HT derivatives include end-group manipulation, block copolymer growth and incorporation of functional pendant groups. Elegant structures can result from well-defined polymer−particle interactions, such as the assembly of CdSe NRs parallel to the long axis of P3HT fibrils by solvent-induced cocrystallization of P3HT with P3HT-functionalized NRs (Figure 2b).[35] In addition to a high fidelity of association between nanowire fibrils and semiconducting NRs, as observed by TEM, a near-complete quenching of the polymer PL suggests an intimate contact between the two species. Although the hybrid fibrils have widths similar to those of standard P3HT fibrils (∼15 nm), their length is truncated significantly due to interruption of nanowire formation by the cocrystalizing polymer ligands. Later studies showed the successful preparation of micron-long hybrid fibril structures by crystallization of P3HT end-functionalized with thiol or phosphonic acid moieties, followed by incubation with CdSe QDs or NRs.[36] TEM characterization revealed both single fibrils decorated with CdSe nanoparticles and multiple alternating parallel lanes of the *p*-type fibrils and *n*-type nanoparticles (that is, 'superhighways,' Figure 2c).

Polythiophene-based diblock copolymers

Diblock copolymers containing polythiophene can have unique, tunable solubility and assembly properties compared with the parent conjugated homopolymers. Such is the case for poly(3-octyl thiophene)-block-poly(ethylene oxide) (P3OT-b-PEO) diblock copolymers prepared by Park *et al.*,[37] in which the assembled structure is controlled by solvent choice and the presence of salt. In a nonselective solvent (tetrahydrofuran), P3OT-b-PEO chains are fully solvated and show orange fluorescence; addition of a solvent highly selective for the PEO block (water) gave spherical aggregates with red fluorescence, while a marginally selective solvent for PEO (methanol) gave fiber-like assemblies with blue fluorescence. The PL intensity of P3OT-b-PEO in water decreased substantially compared to the polymer in tetrahydrofuran, as is typical for π-stacked systems, yet assemblies in methanol showed no decrease in quantum yield. The emission wavelength of the assemblies in methanol also varied with excitation wavelength, indicating that within the fibers, π–π stacking and interchain ordering is distorted, and that segments of planarized polythiophenes vary in length.

Solvent induced fibrillization of P3HT was also used to drive the assembly of all-thiophene block copolymers, in which a functional conjugated block decorates a crystalline core in a coaxial morphology. For example, introducing reactive groups into the noncrystalline polythiophene block gives access to robust cross-linked structures. Primary amines in one polythiophene block enable fibril cross-linking by reaction of the amines with added diisocyanates (Figure 2d); in solvents that normally solubilize P3HT and dissolve fibrils, these cross-linked fibrils maintain their structure, as evident by vibronic

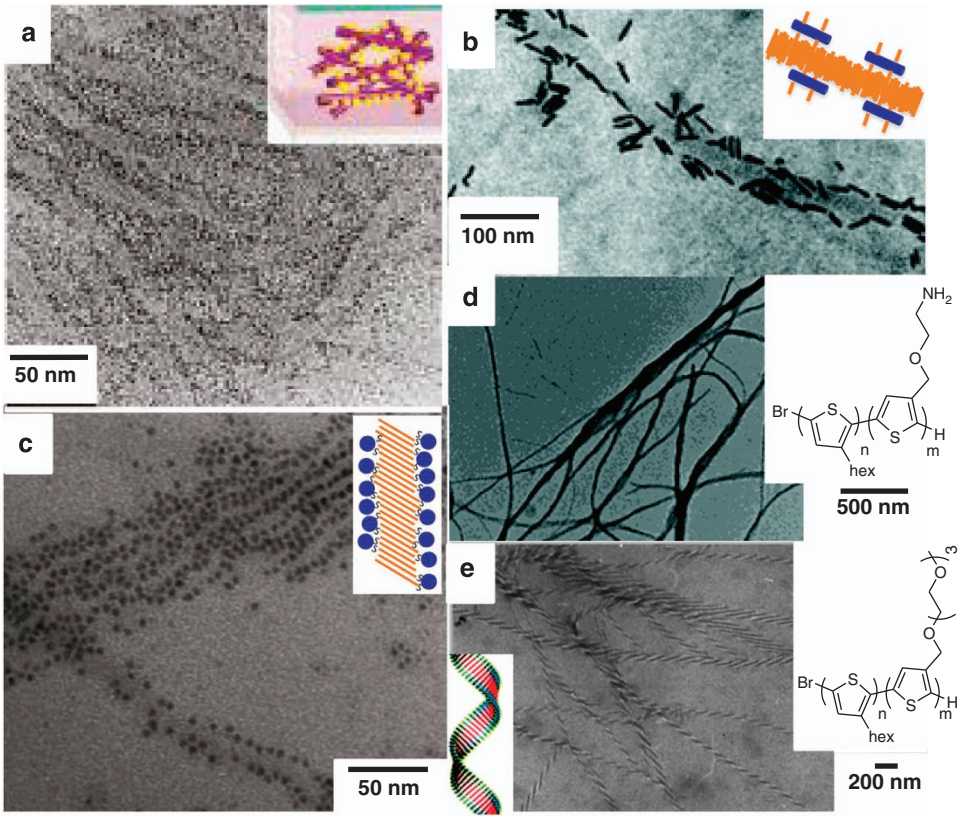

Figure 2 TEM images of: (**a**) CdS-covered P3HT fibrils. Reprinted with permission from Ren *et al.*[34] Copyright 2011 American Chemical Society. (**b**) Cocrystallized P3HT with P3HT-functionalized CdSe NRs. Reprinted with permission from Bokel *et al.*[35] Copyright 2011 American Chemical Society. (**c**) Fibrils of thiol-terminated P3HT with CdSe QDs. Reprinted with permission from Pentzer *et al.*[36] Copyright 2012 John Wiley and Sons. (**d**) Fibrils of P3HT block copolymers, in which one block contains pendant amines, which have been cross-linked by addition of a diisocyanate. Reprinted with permission from Hammer *et al.*[38] Copyright 2011 American Chemical Society. (**e**) Helical P3HT-P3(TEG)T fibrils with KI. Reprinted with permission from Lee *et al.*[39] Copyright 2011 American Chemical Society.

bands in the UV–vis spectrum and TEM.[38] Moreover, cross-linking provided access to nanowires suspended stably in solvents that normally give uncontrolled precipitation, allowing for the manipulation of these extended structures under a variety of conditions. In another example, P3HT-b-P3(TEG)T (triethylene glycol) assembled into fibrils, which upon addition of potassium salts, evolved into helical nanowires $\sim$15 nm in width with a regular pitch of 110 nm.[39] Coassembly of these individual helices gave superhelices, microns in length and up to 150 nm in diameter (Figure 2e). This morphological change occurs to accommodate the steric requirements of the system, as the inner P3HT domain of the fibril retains its crystallinity, and the outer TEG-containing domain contracts upon coordination of K^+.

BUILDING FROM CARBON—FROM SELF-ASSEMBLED SYSTEMS TO GRAPHENE

Polyaromatic hydrocarbons

Polyaromatic hydrocarbons (PAHs), conjugated structures composed of fused aromatic rings, represent a growing class of carbon-based electronic materials. PAHs range in size from small fused-ring structures, such as anthracene, to massive, continuous graphene sheets of interest for novel carbon-based electronic materials and reinforced nanocomposites.[40] Intermediate between these structures are variously sized PAH systems, each seeking to balance performance and processability. Although ideal electronic properties are expected from pure PAHs, their intrinsically poor solubility, due to strong π-stacking interactions, presents processability issues such that external (that is, additives) or internal (that is, covalently attached) processing aids are required. Current efforts towards optimized performance address the synthesis of soluble PAHs of a variety of well-defined sizes (MW) and structures (tailored solubility) capable of solvent-driven assembly into higher ordered structures.

Hexabenzocoronenes: Synthesis and liquid crystalline behavior

Prominent among PAHs is hexabenzocoronene (HBC), a planar, discotic structure composed of 13 fused phenyl rings. HBC and its derivatives are synthesized by Diels–Alder cycloaddition of pentaphenyl–cyclopentadienone with diphenyl acetylene, giving an oligophenylene that transforms to the fused structure upon oxidation (Figure 3a).[40] HBCs are liquid crystals (LCs), π-stacking in solution to form columns, which may provide ideal percolation pathways for charge transport between electrodes in PV devices (Figure 3a).[41] Aliphatic chains solubilize the individual molecules and resulting structures, and dictate the LC phase transition temperature by reinforcing columnar stacking through solvophobic interactions. HBC columns exhibit excellent photoconduction ($1\,cm^2\,V^{-1}\,s^{-1}$) when oxidatively doped (for example, with nitrosonium tetrafluoroborate),[42] and provide electron or hole transport in the active layer of a bulk heterojunction PV device. The highest occupied molecular orbital/ lowest unoccupied molecular orbital

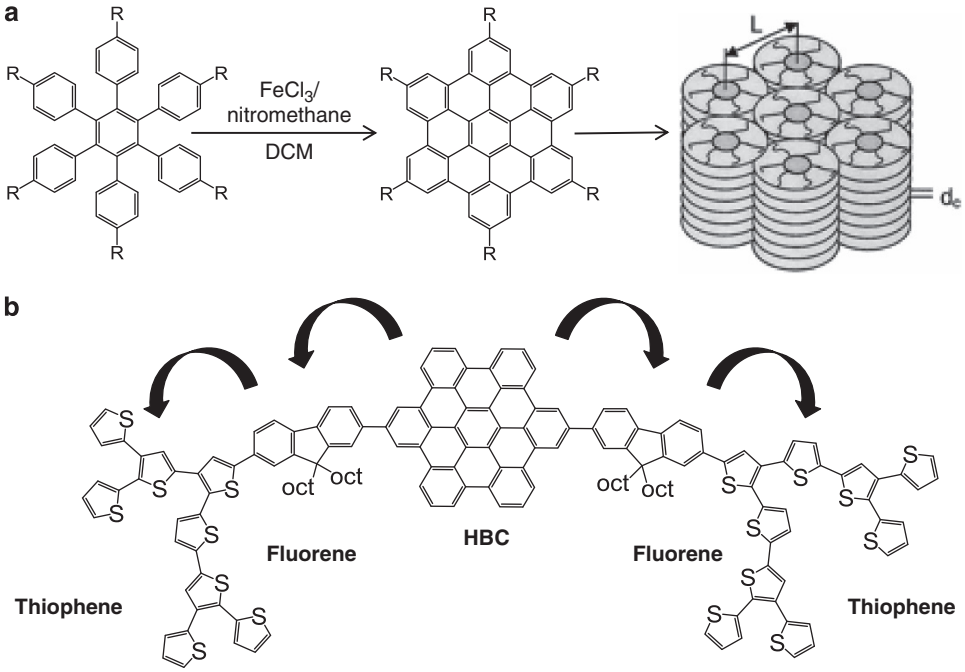

Figure 3 (**a**) Synthesis of alkylated HBC and its assembly into columnar LCs by π–π stacking. Reprinted with permission from Schmidt-Mende *et al.*[42] Copyright 2001 The American Association for the Advancement of Science. (**b**) HBC-fluorene-branched thiophene triads designed for electron transport (indicated by the arrows) from the HBC core to the thiophene ends.

(HOMO/LUMO) energies of HBC (−5.25/ −2.64 eV) trend towards its use as an electron donor, while the large band gap (2.9 eV) necessitates blending with lower band gap materials to provide absorption over an appreciable wavelength range.

Seminal work on HBC-based PV devices combined HBC LCs for hole transport, with perylene diimide (PDI) for electron transport, and showed nanoscale vertical phase separation of the two components in thin films by electron microscopy.[42,43] Interestingly, the presence of HBC LC columnar stacks disrupted the tendency of PDI to form large (micron scale) crystals, and led to the formation of interconnected nanoscale domains of the two materials. PDI fluorescence was quenched due to photoinduced charge separation, and devices with a power efficiency maximum of nearly 2% were obtained upon irradiation at 490 nm. Thermal annealing following deposition of a removable polydimethylsiloxane stamp proved beneficial to lower the surface roughness of the film, facilitate vertical stratification, prevent the formation of pinholes and improve device performance.[44] The open circuit voltage increased from 0.55 to 0.7 V, and the external quantum efficiency at 460 nm increased from 22 to 30%. HBCs with short, branched alkyl side chains gave the best vertical phase separation of the active layer (interpenetrated nanodomains), as determined from cross-sectional scanning electron microscopy (SEM) images. Moreover, HBC with shorter branched alkyl chains acted as the best donor for PDI, translating into the highest external quantum efficiency (12% at 460 nm, compared with $<6\%$ for HBCs with linear solubilizing chains).

Influence of side chains on HBC assembly

HBC assembly is exquisitely sensitive to the structure of the alkyl side chain, as reflected in association constants determined by UV–vis, PL, PL emission, and ^{1}H nuclear magnetic resonance (NMR) spectroscopies. Smaller association constants were found for HBCs bearing branched substituents compared with linear ones (for example, 13.4 K_a l mol^{-1} for 2-ethyl hexyl vs 898 K_a l mol^{-1} for dodecyl in tetrachloroethane at 30 °C).[45] Longer side chains reduced HBC association, while *t*-butyl substitution led to essentially no association due to steric constraints. Transferring solution-assembled HBC columns with linear alkyl chains to thin films proved facile, while HBCs containing branched chains gave columnar structures only when cast from a high boiling solvent (for example, xylene). Regardless of the HBC substituents, homogeneous films of microfibers oriented parallel to the underlying substrate were obtained by slow withdrawal of a carbon-coated glass substrate from a toluene solution of HBC; the meniscus formed at the air/liquid interface allowed for HBC crystallization onto the moving support, such that solution-formed HBC aggregates organized into larger anisotropic structures.

HBC assembly is also influenced by the presence of side chain chirality and substitution pattern around the structure. Mullen and co-workers[46] prepared HBCs having a variety of chiral or racemic branched side chains, discovering that branching increased HBC solubility and enabled a tuning of the phase transition temperature to provide LC behavior at room temperature. HBC with chiral side chains had a phase transition temperature distinct from their racemic counterparts, and a circular dichroism-couplet at 249 and 218 nm, reflecting chirality of the HBC columns. Alternating hydrophobic and hydrophilic substituents in C-3 symmetry led to similar assembly trends as other HBC molecules, such as higher crystallinity for linear substituents over branched, and LC behavior over a wide temperature range with a phenyl linker between the alkyl chain and core.[47] Indeed, this phenyl spacer gave HBC columns that persisted upon heating, revealing extended fibrous or rod-like nanostructures by SEM and TEM.

Although π–π stacking drives HBC columnar assembly, intra- and inter-columnar secondary forces, such as hydrogen bonding, can

disrupt or reinforce these structures. The LC behavior of HBC derivatives bearing five 3,7-dimethyl octyl substituents and either butyric (C4) or undecanoic (C11) acid side chains were studied.[48] The phase transition temperature of C11 HBC did not change compared with the alkyl derivative, preserving the hexagonal crystal structure. In contrast, C4 HBC molecules exclusively formed an orthorhombic, higher melting crystal (221 vs 70 °C). This is attributed to intermolecular hydrogen bonding rather than a defined distance between two HBC units, as HBC dimers tethered covalently through an ester or amide linkage did not give the same structural change. The amide-linked HBCs showed no long range order, but the ester-linked molecule showed an unstable pseudocrystalline phase, caused by back folding of the tethered discs. Thus, to reinforce the stacked structures, dynamic interactions afforded by hydrogen bonding act synergistically with π–π stacking of the aromatic core.

The effects of intracolumnar hydrogen bonding were examined using HBC derivatives with an amido or ureido moiety between the core and alkyl chains.[49] These functionalities promoted column formation in solution, working cooperatively with π–π stacking forces. The influence of hydrogen bonding was temperature dependent, with the less hindered and stronger H-bonding compounds showing greater reinforcement (that is, more thermally stable). Notably, direct translation of the solution-assembled structures to the bulk state was nontrivial, and the geometry of intracolumn hydrogen bonding dictated column formation on a solid substrate.

To date, HBC molecules in PV devices suffer from nonidealized exciton dissociation owing to the presence of insulating alkyl chains and column orientation parallel to the substrate, which prevents charge transport directly to the electrodes in a sandwich device geometry. Friend and co-workers[50] used oriented thin films of poly(tetrafluoroethylene) to achieve parallel orientation of HBC columns on the underlying substrate. Orientation normal to the underlying substrate (face-on, Figure 3a) would optimize charge transport in PV devices, and could provide a scaffold to prepare the desired percolated morphology of *p*- and *n*-type domains. Slow crystallization from an isotropic state gave homeotropic (face-on) arrangement of HBC columns between two polar surfaces, as characterized by 2D wide-angle X-ray scattering, though film thickness was limited owing to competing column assembly in solution.[51] This organization of HBC columns is preferred thermodynamically, and growth was likely nucleated by organized face-on monolayers. Furthermore, an ester linkage in the side chain facilitated homeotropic alignment on aluminum or glass surfaces due to affinity of the HBC face for the surface.

In the tandem self-assembly of HBC donor and acceptor, HBC-anthraquinone dyads were synthesized and their homeotropic alignment studied.[52] Assembly of HBC bearing five alkyl substituents and one anthraquinone moiety on graphite led to void defects in long range order, as revealed by scanning tunneling microscopy. This sharply contrasts the well-organized, defect-free hexagonal arrangement observed for HBC-dimethoxyanthracene dyads or HBC molecules bearing six anthraquinones. Hence, HBC packing is not disrupted by covalent attachment of the acceptor, but rather by donor −acceptor interactions in solution or competitive interactions between the graphene surface and donor or acceptor.

HBC-based triads for electron transfer

Holmes[53] reported donor-acceptor HBC triads with coronas that are both solubilizing and electronically active, of potential advantage in solar cells due to increased light absorption and available mechanisms for charge separation. HBCs containing pseudo-ortho or pseudo-para dialkyl fluorene groups were functionalized covalently with oligo(triarylamines) at the fluorene moiety, providing a triad set up for electron flow. Orbital mixing in these structures was evident by quenching of triarylamine PL and shifts in HOMO/LUMO energies upon conversion from the dyad (−5.8/ −3.2 eV) to the triad (−4.7/ −2.1 eV). However, PV devices containing active layers of triad with fullerenes gave PCEs of only 0.22%; while these values are similar to those reported for other HBC-containing solar cells, this system showed improved stability under more intense illumination.

Self-assembled HBC-fluorene-branched oligothiophene triads (Figure 3b) showed that, upon assembly of the HBC core, the thiophene units offset one another to accommodate steric demands.[54] Two-dimensional (2D) wide-angle X-ray scattering showed the same inter-HBC separation (0.35 nm) for columns of the triad as core only, but additional reflections were observed for the HBC-fluorene-branched oligothiophene columns, which indicate a complex helical packing. PV devices containing these triads and $PC_{71}BM$ as the active layer gave a PCE of 2.5%, ∼5 times higher than the devices consisting of the branched oligo(thiophene)s without the HBC core. Atomic force microscopy (AFM) characterization showed distinct nanoscale phase separation of the HBC-containing compounds and fullerene, suggesting that columnar stacks facilitate direct hole transport.

Nanotubes and nanocoils from amphiphilic HBC

Synthetic methods that differentiate HBC into hemispheres offer an opportunity to prepare unique self-assembled structures. Aida and co-workers[55] showed that amphiphilic HBCs (having a mini Janus plane, Figure 4a) have distinctly different assembly properties than HBCs with any other substitution pattern. Specifically, HBCs bearing two pseudo-cis alkyl chains and two pseudo-cis TEG chains self-assemble into hollow nanotubes by π-stacking in tetrahydrofuran. The 3 nm thick nanotube walls are composed of a bilayer of molecules, in which the outer and inner surfaces are lined with TEG chains, and the alkyl chains localize to the center of the wall (Figure 4b). These structures are thermally stable up to 100 °C and upon oxidizing with nitrosonium tetrafluoroborate, convert from insulator to semiconductor with a resistivity of 2.5 MΩ at 285 K. Processing techniques common to polymers were applied to these nanotubes: pulling nanotube bundles from solution with a glass hook gave fibers 5–30 mm long and 0.5–5 mm wide, in which the long axis of individual HBC columns is parallel to the macrofiber long axis, ideal for charge transport along the fiber.[56] Indeed, these fibers revealed semiconductor behavior upon doping with iodide, and resistivity parallel to the fiber axis (20 Ωcm) was much lower than that perpendicular to the fiber axis (280 Ωcm).

During the assembly of amphiphilic HBC molecules into nanotubes, nanocoil structures were observed as kinetic intermediates (Figure 4c), though all nanocoils converted to nanotubes upon heating or oxidative doping. Stabilizing these nanocoils by chemical cross-linking is interesting for producing stable, single-handed nanocoils with applications as helical electron conductors and nanosolenoids. To this end, nanocoils formed from amphiphilic HBC molecules bearing a norbornene moiety on the TEG chain end were stabilized by ring opening metathesis polymerization (ROMP) of the norbornene, giving nanocoils that proved stable to heat and doping, with conductivity values of $\sim 10^{-4}$ S cm^{-1}.[57] Nanocoils of controlled, homogeneous handedness were obtained by assembly of the norbornene-functionalized amphiphilic HBC molecule in which 20 mol% of the molecules contained a chiral center on the TEG chain.[58] Cross-linking by ROMP led to batches of

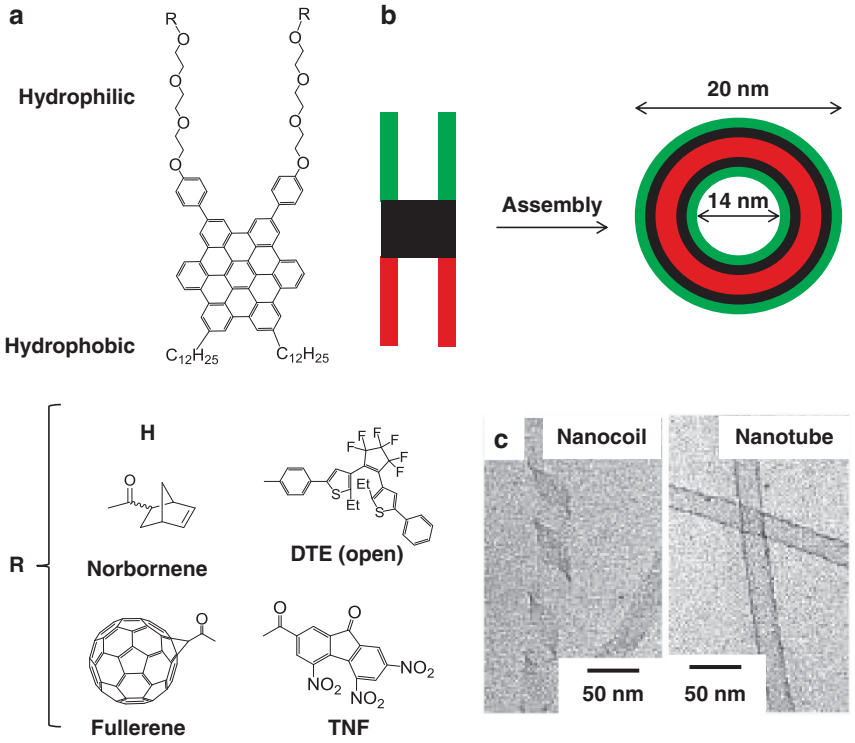

Figure 4 (**a**) Amphiphilic alkyl/glycol substituted HBCs and the R groups used to functionalize the TEG chain end. DTE = dithienylethene. TNF = trinitrofluorenone. (**b**) Representation of the assembly of amphiphilic HBC into a nanotube, in which the walls contain a bilayer of molecules with TEG chains lining the inner and outer walls. (**c**)TEM images of nanocoil (left) and nanotube (right). Reprinted with permission from Hill *et al.*[55] Copyright 2004 The American Association for the Advancement of Science.

nanocoils of a single handedness, which were 30 nm in diameter, 60 nm in pitch and 20 nm in tape width.[57]

Donor–acceptor HBC nanotubes

Covalent attachment of trinitrofluorenone (TNF) to the TEG chain end of amphiphilic HBC resulted in quenching of HBC PL due to electron transfer from HBC to TNF.[59] In solution, amphiphilic HBC with one TNF group (Figure 4a) formed nanotubes, which exhibited photocurrent under irradiation without the need for doping. By coassembly of the TNF and non-TNF functionalized HBC derivatives, TNF density was tuned and it was homogeneously distributed throughout the nanotube, as determined by a shift in phase transition temperatures. Even at low incorporation of HBC–TNF, a dramatic reduction in HBC fluorescence was observed (80% reduction at only 10 mol% HBC–TNF).[60–62] Moreover, the spatial separation between the inner, electron-donating HBC domain and outer electron-accepting TNF molecules prevented rapid charge recombination of electron and hole after exciton dissociation, as the lifetime of photogenerated charge carriers was independent of TNF content. Photoconductivity of the nanotubes showed a bell-shaped dependence on TNF content, reaching a maximum ($3.5 \times 10^{-2}\,cm^2\,V^{-1}\,s^{-1}$) at 75% TNF–HBC, and decreasing at higher TNF content due to disrupted π–π stacking.

To extend the utility of amphiphilic HBC assembly by controlling photoconduction, Aida and co-workers[63] functionalized one of the TEG chains with dithienylethene (DTE, Figure 4a), a thermally stable molecule that undergoes reversible light-induced cyclization. Dramatic differences in photoconductivity were observed for nanotubes containing open and closed DTE states. Field effect transistor and flash photolysis time-resolved microwave conductivity showed an order of magnitude higher conductivity for the closed form over the open structure (4.9×10^{-3} vs $9.6 \times 10^{-4}\,cm^2\,V^{-1}\,s^{-1}$), attributed to better electron transfer in the planar closed form. Additional impressive structures arose from the assembly of amphiphilic HBCs containing a fullerene-substituted TEG chain, giving coaxial nanotubes with inner and outer surfaces covered with fullerenes. Although these nanotubes displayed unbalanced ambipolar charge transport (10^{-5} for electrons and 10^{-7} for holes), coassembly of the HBC-fullerene with the non-fullerene analog served to balance charge mobilities, demonstrating the modular and tunable nature of this innovative design.

In addition to a coaxial alignment of *p*-type (HBC) and *n*-type (TNF, dithienylethene, fullerene) moieties, nanotubes with segmented *n*- and *p*-type domains, that is, block nanotubes, were prepared by stepwise assembly of two HBC derivatives (Figure 5).[64] Diblock and triblock nanotubes were formed by the growth of electronically deficient fluoride-substituted HBC amphiphiles from seed crystals of preassembled amphiphilic HBC molecules bearing bipyridyl groups that were coordinatively cross-linked with copper cations. These structures displayed excitation energy transfer between the different nanotube domains and longer lived charge carriers than the parent homogeneous nanotubes, indicating charge separation between the two domains within the nanotube.

Higher-order PAHs

Although HBC derivatives exhibit impressive self-assembly features and electronic properties, the synthesis and use of higher-order PAHs (Figure 6) could provide access to improved electronic properties and supramolecular assemblies, though synthetic complexities and limited

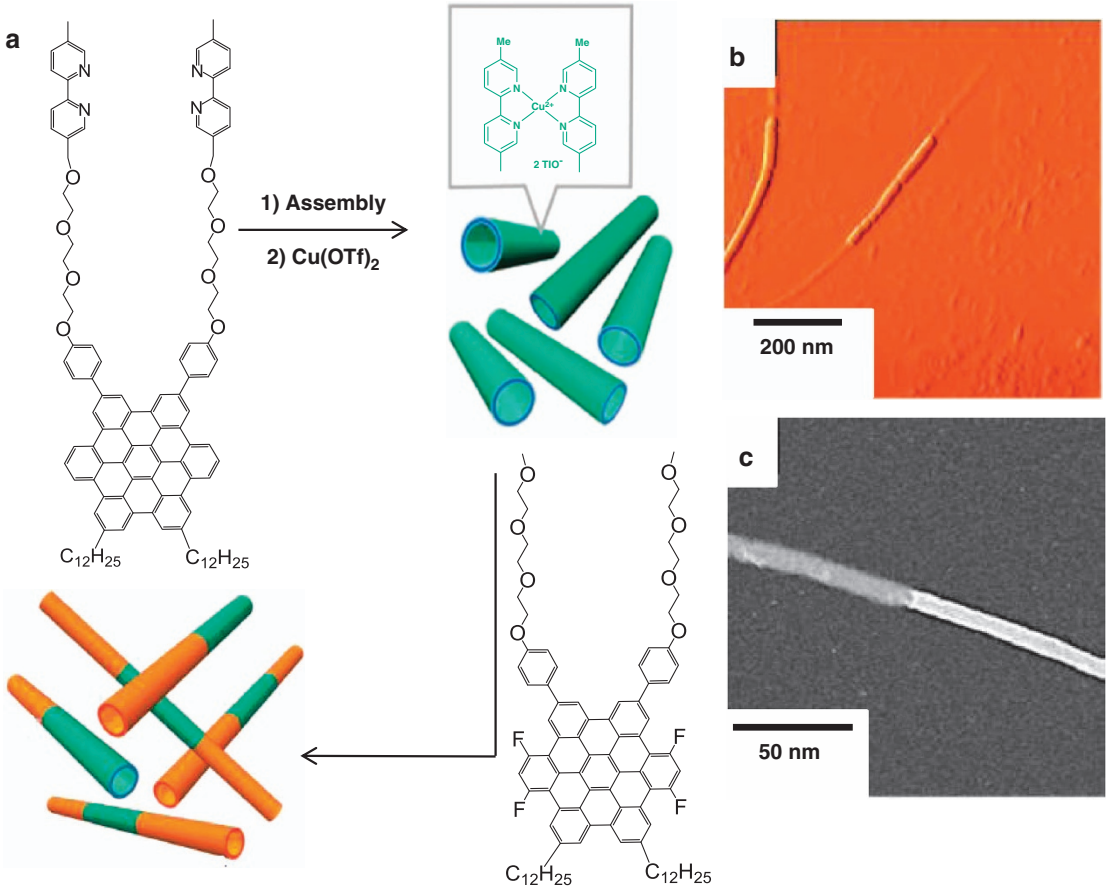

Figure 5 (**a**) Assembly and cross-linking of bipyridyl-containing HBC and their use as seeds to grow a second block of electron-deficient HBC. (**b**) Tapping mode atomic force micrograph of block nanotubes; (**c**) Scanning TEM of block nanotubes. Reprinted with permission from Zhang *et al.*[64] Copyright 2011 The American Association for the Advancement of Science.

solubility have prevented their widespread application. Phenyl-based AB_2-type monomers undergo Suzuki coupling to give globular hyperbranched polyphenylenes that can be combined with organic small molecules[65] or surface-functionalized for tailored applications.[66] By the $FeCl_3$ dehydrogenation of dendritic polyphenylene, Mullen and co-workers[67] achieved the preparation of PAHs much larger than HBC. The geometry of the initial polyphenylene dendrimer strongly influenced product distribution, as dehydrogenation started independently on each dendron arm and proceeded to the core. At a critical degree of dehydrogenation a propeller-like conformation of the molecule geometrically prevented the arms from reacting with the phenyl core, precluding complete planarization of the system.

Extending the higher-order PAH concept, pure 'nanographene' sheets containing a planar aromatic core of 132 carbon atoms (50 fused 6-membered rings) with eight solubilizing branched alkyl substituents was synthesized. Nanographene fibers over 10 μm in length, 16 nm in width and 12 nm in height were obtained on mica from trichlorobenzene.[68] Nanographene composed of 222 carbon atoms (37 fused benzene rings, Figure 6a), without solubilizing substituents was prepared by oxidation of the precursor polyphenylene using $Cu(OTf)_2$ and $AlCl_3$ at 30 °C for 1 day.[69] The product was insoluble due to the lack of side chains, but its structure was confirmed by solid state ^{13}C NMR and MALDI-TOF.

Recent synthetic efforts have generated nanographene with D2 symmetry, distinct from the well-studied C6-symmetric HBCs.[70] This oval shaped 'nanographene,' consisting of 45 carbon atoms (15 fused rings) bearing six alkyl groups, self-assembled into columnar stacks, in which neighboring molecules were offset by 90 degrees. The bottom-up synthetic limits for nanographene were pushed further by the Suzuki coupling of oligophenylene moieties to give hyperbranched polyphenylene, which underwent intramolecular oxidation using $FeCl_3$ to yield 2D ribbon-like nanographene.[71] Scanning electron microscopy characterization showed that 1D nanoscale objects, ~100 nm in diameter and several microns in length, were obtained after drop-casting a tetrahydrofuran solution of these polymers onto a Si substrate. Scanning tunneling microscopy analysis at the *n*-dodecane/HOPG interface showed parallel nanoribbons, suggesting a face-on arrangement on the HOPG surface.

Complementary to these bottom-up approaches that provide precise control over the size and substitution pattern of PAHs, a top-down approach to such structures by 'oxidative cutting' of carbon fibers has yielded π-stacked PAHs, termed graphene nanoparticles.[72] These structures are 2–3 nm in diameter, have two or three π-stacked PAH moieties comprising the core, and an oxygen-rich corona.[73] The optical properties of these structures are highly dependent on particle size; the absorption maxima red-shifts with increased particle size, while emission wavelength depends on the excitation energy, possibly due to variation in the density of defect sites associated with sp^2 carbons.

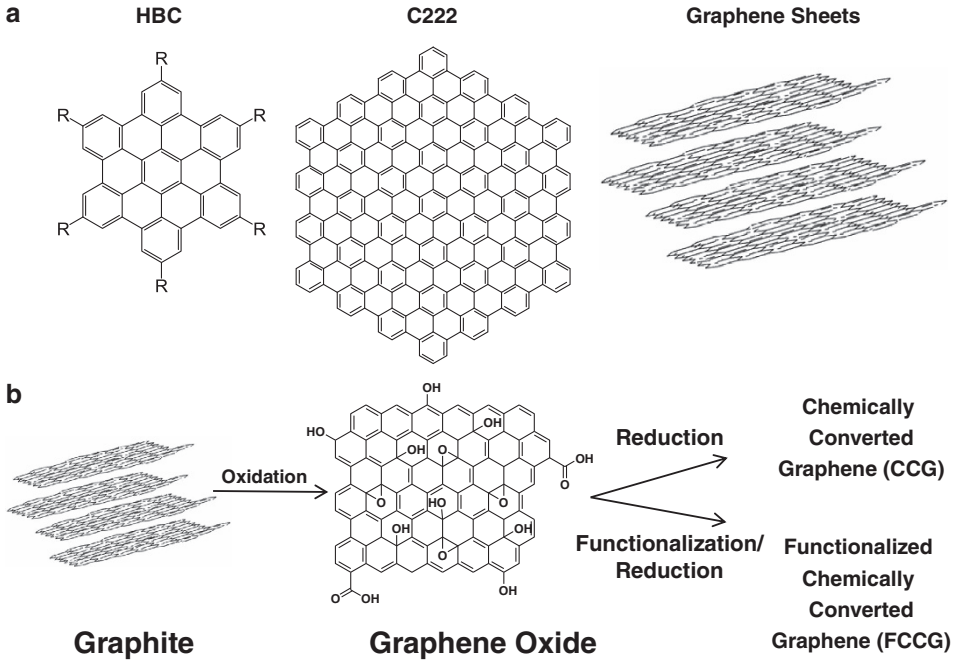

Figure 6 (**a**) Progression of PAHs from HBC to graphite. (**b**) Manipulation of graphite for the preparation of nanocomposites: oxidation of graphite to GO and the routes to CCG and FCCG.

Functionalized graphene and its integration into hybrid materials

Distinct from smaller PAHs, graphene itself is an extended 2D monolayer sheet of sp^2-hybridized carbon with excellent conductivity and mechanical properties.[74,75] As with other extended sheet-like structures, such as montmorillonite clay,[76] graphene is considered an ideal additive for composite materials, contributing mechanical properties at extremely low weight percent loading. However, unlike clay, graphene offers the added benefit of high conductivity.[74,77,78] Indeed, the percolation threshold of graphene sheets in polymer materials is very low, generally <0.2 vol% platelet incorporation creates a percolated network through an insulating matrix, which translates to conductivity values that are orders of magnitude higher than the polymer itself. Unfortunately, strong inter-sheet attractions hinder processability and the facile preparation of graphene nanocomposites. Attempts to overcome these limitations harness chemistries that improve graphene solubility and its interactions with the surrounding matrix, for example, polymers, nanoparticles, etc.

While initial reports of graphene composites focused on their electrical and mechanical properties, recent interest has expanded to other applications. Graphene for metamaterials and plasmonics has recently been examined theoretically,[79] and graphene-based materials are the key components of numerous materials and devices, including batteries, which harvest ionic thermal energy,[80] foams for light-weight electrodes,[81] and composites for thermal interface materials.[82] Moreover, coassembly of graphene with QDs has been used to generate multiple charge carriers from a single incident photon,[83] while ink-jet printing[84] and roll-to-roll processing techniques[85] advance graphene-based materials towards commercialization.

Interest in graphene analogs parallels efforts on graphene itself. For example, the preparation of the silicon analog of graphene, termed silicene,[86] demonstrates that other 2D lattices can have Dirac points (where the valence and conduction bands meet in a single point at the Fermi level) that impart graphene-like conductivity. Theoretical studies suggest that graphynes,[87] frameworks containing all sp^2-hybridized carbons bridged with alkynes, should have similar electronic properties to graphene as well. Recent advances in the patterned or complete fluorination of graphene allow the electronic properties and solubility of the carbon framework to be tailored, giving rise to insulating sheets a single carbon layer thick for use as interlayers in electronic applications.[88,89]

Graphene modification and processing

The most common method for preparing soluble, functionalizable graphene derivatives is the preparation of individual sheets of graphene oxide (GO) by the treatment of insoluble graphite (that is, aggregated graphene platelets) with strong acid. GO has a disrupted π-system (similar to acid-treated carbon nanotubes), a crumpled carbon framework bearing hydroxyl and epoxide groups on sp^3 hybridized carbon atoms within the sheet, carboxylates along the edges, and a C:O ratio of ~2:1 (Figure 6b).[90] Although the electronic properties of GO are diminished greatly compared with graphene, improved dispersibility allows their incorporation into composites. GO can be directly intercalated with hydrophilic polymers, such as poly(vinyl alcohol) and poly(ethylene oxide), while composites with hydrophobic polymers, such as polystyrene (PS) are achieved by polymerization in the presence of GO,[91] or by grafting from the graphene surface.[92]

Thermal or chemical reduction of GO within a polymer matrix restores the π-conjugation of platelets, giving 'reduced GO', which has a C:O ratio of 10:1, indicating residual defects as a result of incomplete reduction.[93] Recent work seeks to maintain the pristine graphene framework while accessing exfoliated, single graphene sheets by selective edge-functionalization using Friedel–Crafts acylation,[94] and by recovering conductivity through mild conditions, such as flash photolysis.[95] Highly water soluble, processable graphene has been prepared by the partial reduction of GO, followed by functionalization and further reduction.[96]

When incorporating graphene or reduced GO into polymers for enhancing conductivity, surface functionalization is crucial for balancing graphene dispersion with electronic performance. Chemically converted graphene (CCG) sheets result from the reduction of unfunctionalized GO, whether or not in the presence of a polymer matrix. Alternatively, functionalized chemically converted graphene (FCCG) is obtained when GO is reduced after undergoing covalent modification with a polymer or small molecule, commonly by the reaction of GO hydroxyl groups with isocyanates.[97] In FCCGs, permanent sp^3 carbons present within the sheet preclude full recovery of the electronic properties of pristine graphene. Nonetheless, the processability afforded by this functionalization-reduction approach is practical and effective in forming composite materials with a variety of polymers. Worth noting is the influence of the starting carbon-based material and reaction conditions on the resulting properties of GO; nanometer-sized GO platelets prepared by the oxidation of graphene nanofibers remained stable in solution after hydrazine reduction, in contrast to microns-width GO sheets prepared from graphite powder.[73]

The covalent functionalization of GO with phenyl isocyanate, followed by blending with PS and reduction of GO with dimethylhydrazine at elevated temperatures was reported by Ruoff and co-workers;[97] the urethane linkages remained after reduction, and the resulting composites exhibited conductivity similar to carbon nanotube-PS composites ($0.12\,S\,m^{-1}$), but at a lower percolation threshold ($\sim$0.1 wt%) compared with carbon nanotubes ($\sim$0.3 wt%). In a composite of phenyl-decorated FCCG and PS, the spin-coating rate strongly influenced orientation of the platelets in thin films. At slower rates (600 r.p.m.), platelets aligned perpendicular to the underlying substrate and protruded from the film surface, a desirable orientation for charge transport in sandwich device constructs, though at the cost of increased surface roughness. Dodecyl-substituted FCCG proved well-suited for blending with high volume engineering plastics such as linear low density polyethylene: the electrical resistivity decreased from $10^{16}\,\Omega$cm for pure linear low density polyethylene to 10^7 and $10^4\,\Omega$cm at 3 and 8 wt% FCCG, respectively.[98]

Chung and co-workers [99] reported PS/CCG composites prepared without covalent modification to the graphene; sonication of a methanol solution of CCG with PS gave a colloidal suspension, which upon filtration, produced composite pellets with high conductivity ($>70\,S\,m^{-1}$) at $\sim$2.5 vol% graphene, and dramatic improvement in the thermal stability of PS. These composites were intrinsically hole doped, having *p*-type characteristics at higher temperatures, with field effect transistor mobilities 2–5 times higher for holes ($0.1–1\,cm^2\,V^{-1}\,s^{-1}$) than electrons. Moreover, Zhang and co-workers[100] compared the conductivity of poly(vinyl chloride)/poly(vinyl acetate) with CCG and exfoliated graphite (the graphite was sonicated to mechanically separate the sheets); at loadings below 1.5 vol%, the CCG composites gave electrical conductivity three to five orders of magnitude higher than those with expanded graphite (10^{-4} vs $10^{-8}\,S\,cm^{-1}$), showing that better dispersion of CCG gave percolation.

GO at interfaces

Interfacial and surface localization of graphene opens opportunities for concentrating the conductive material into continuous structures at precisely defined locations. For example, hydrazine reduction of GO in a water/EtOH dispersion with polyethylene particles gave a continuous CCG shell on the particles at $<$0.1 vol% graphene.[101] Dramatic improvements in conductivity were observed upon small increases in CCG content, from 10^{-8} to $10^{-4}\,S\,m^{-1}$ for 0.06 −0.076 vol%, plateauing at $10^{-1}\,S\,m^{-1}$ at 0.6 vol% CCG. Interestingly, thermal annealing completely disrupted conductivity, as diffusion of CCG into the polymer destroyed the percolated network of graphene.

The inherent amphiphilic or surfactant nature of GO affords segregation to air −liquid and liquid −liquid interfaces, as pioneered by Huang and co-workers.[102] Pickering-type oil-in-water emulsions, so-called 'armored droplets,' formed upon adding an organic solvent to an aqueous solution of GO, while GO segregation to the air −water interface was studied by Langmuir −Blodgett techniques.[103,104] Langmuir −Blodgett films of single GO sheets (one carbon atom thick) were reduced to give CCG films with a resistance of 4 MΩ cm, similar to values obtained for multilayer CCG films.[103] The assembly properties of GO were controlled further by tuning the pH and platelet aspect ratio (thus, varying the amphiphilicity of the structures).[105–107]

Graphene composites exploiting π–π interactions

Exploiting π–π interactions between graphene and other aromatic molecules during synthesis can effectively organize materials that are otherwise not processable. One such class of novel, innovative materials is seen in 2D porous covalent organic frameworks prepared by the condensation of aromatic hydroxyl- and boronic acid-rich structures (Figure 7a), and isolated as crystals of π-stacked sheets.[108] By synthesizing these materials in the presence of a single layer of graphene on a substrate, Dichtel prepared graphene surfaces functionalized with one or a few covalent organic framework (COF) sheets, in which the pores of the COF oriented normal to the surface (Figure 7b).[109] Better long range order improves the crystallinity of the COF on graphene relative to solution-assembled COFs, and direct routes for charge transport through the COF to graphene become apparent. This method works to assemble various COFs with pore sizes up to 4.7 nm, giving tubular pores that can be filled with complementary electronic materials, such as fullerenes, to give percolated networks ideal for PV applications.[110] Indeed, assemblies of covalent organic frameworks containing phthalocyanates, materials with proven utility in PV devices, show strong UV–vis absorption and are highly photoluminescent, suggesting that filling of the COF pores with a complimentary material could produce efficient devices.

Small molecules capable of multidentate interactions can also be assembled into highly stable monolayers on a single layer of graphene on a substrate. One such molecule, a tetrapod with three pyrene (Py) arms for promoting strong interaction with a graphene surface and a redox-reactive Co(II) bis-terpyridyl, forms monolayers with no aggregation of the terpyridyls, which extend normal to the surface (Figure 7c).[111] These multifunctional monolayers were stable for hours at infinite dilution, in contrast to analogs bearing only one Py moiety, which desorbed rapidly from the graphene surface in organic solvents.

π–π interactions can also be harnessed by reducing solution suspended GO in the presence of π-conjugated polymers to prepare conductive, processable graphene composites. For example, Zhang and co-workers[112] formed sandwich-type structures, in which the aromatic block of coil-rod-coil polyethylene glycol-poly(phenylene ethynylene)-polyethylene glycol triblock copolymers interact with graphene, giving non covalently 'tethered' PEG chains that improve processibility and provide solubility in polar solvents at orders of magnitude higher concentration than CCG alone. This approach was also used to prepare stable composites with high conductivity by

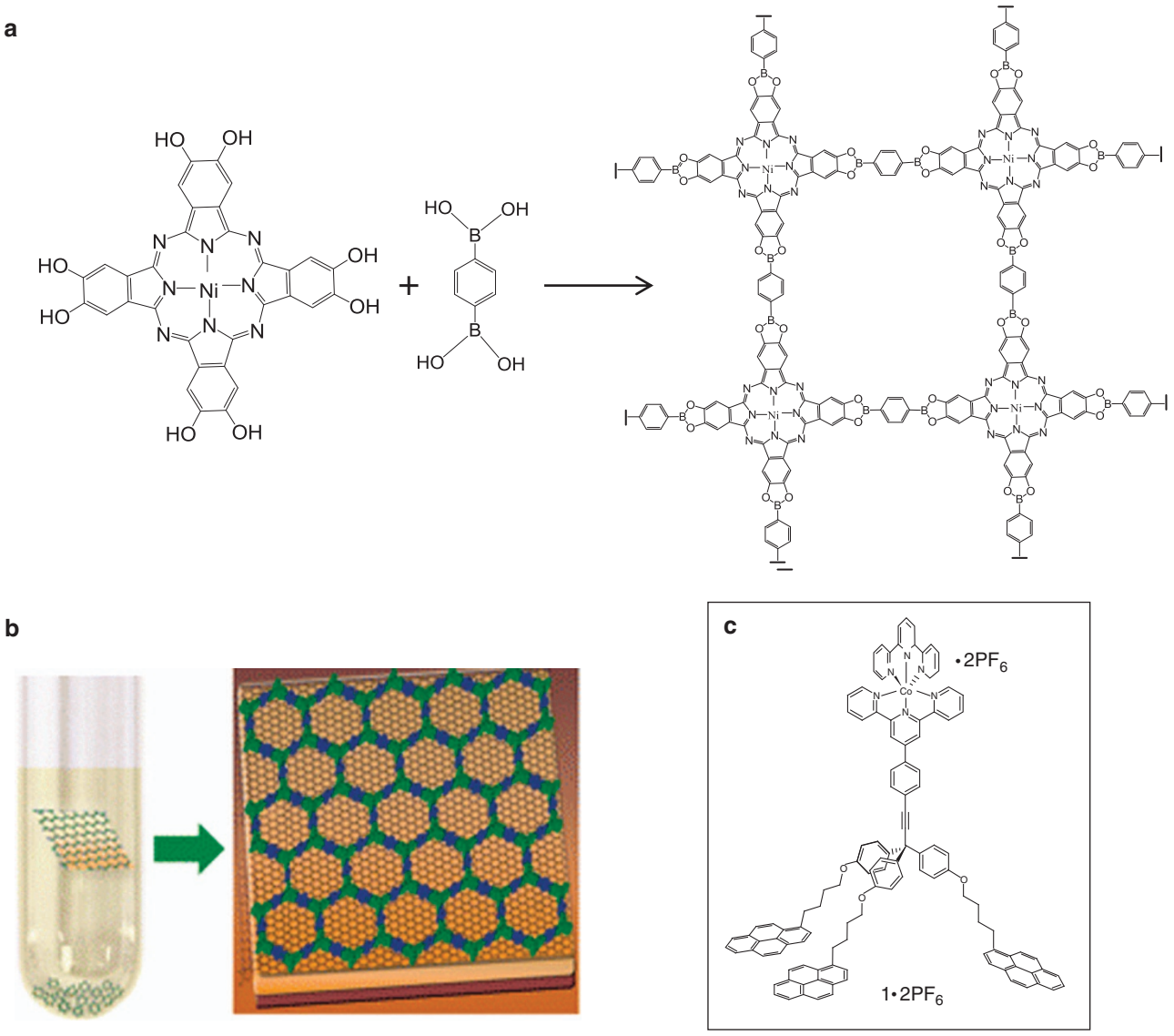

Figure 7 (**a**) Solvothermal synthesis of Ni phthalocyanine-containing COF; (**b**) The presence of graphene during COF synthesis leads to COF deposition onto graphene. Reprinted with permission from Colson *et al.*[109] Copyright 2011 The American Association for the Advancement of Science. (**c**) Molecule that multivalently binds to graphene through three pyrene arms. Reprinted with permission from Mann *et al.*[111] Copyright 2011 American Chemical Society.

hydrazine reduction of GO in the presence of sulfonated polyphenylene ethylene.[113] Water soluble structures resulted from interactions of the aromatic phenylene−ethynylene backbone with the CCG, giving composite thin films with comparable resistivity to CCG, in contrast to composites of CCG with poly(sodium 4-styrenesulfonate) or poly(vinyl pyrrolidone), each having a saturated backbone. Notably, GO itself can facilitate the aqueous dispersion of single walled carbon nanotubes by π–π interactions between the partially oxidized basal plane of GO and the aromatic carbon nanotubes walls. These hybrid structures were combined with C_{60} to afford an all carbon active layer in PV devices with an impressively high open circuit voltage of 0.59 V.[102] Recently, Bao and co-workers[114] reported all carbon bilayer PV devices, having an active layer of poly(3-alkylthiophene)-wrapped single-wall carbon nanotubes and C_{60}. Although a PCE of 0.46% was obtained using standard metal electrodes, devices fabricated with an anode of CCG, and cathode of n-doped single-wall carbon nanotubes, gave a PCE of 0.006%, likely owing to contact resistance between the electrodes and active layer, but nonetheless demonstrating the feasibility of all carbon solar cells.

Mullen and co-workers[115] exploited π–π interactions between CCG and anionic derivatives of Py, electron donor and PDI, electron acceptor to give processable CCGs. The formation of Py−CCG and PDI−CCG charge transfer complexes was verified by X-ray photoelectron spectroscopy and Raman spectroscopy. Thin film conductivity measurements revealed an increase in charge mobility for CCG−PDI (13.9 S cm^{-1}) compared with CCG (3.0 S cm^{-1}) and CCG−Py (1.9 S cm^{-1}). Upon thermal annealing of the samples at 1000 °C, the conductivity of pure CCG (517 S cm^{-1}) was substantially lower than CCG−PDI (1314 S cm^{-1}) and CCG−Py (1149 S cm^{-1}), attributed to healing of defects in the carbon framework by the adsorbed π system.

Additional intercalation strategies seek to polymerize monomers in the presence of GO or CCG platelets which circumvents covalent

modification of the all-carbon structures, but introduces numerous challenges such as graphene sedimentation during polymerization. However, recent reports by Li and co-workers[116] note that fast and efficient microwave-initiated polymerization of polyethylene glycol−methacrylate maintained GO dispersion during polymerization. Porous hydrogel composites were obtained using GO sheets as 2D templates during the preparation of polyaniline, polypyrrole and poly(3,4-ethylenedioxythiophene).[117] The GO/polypyrrole hydrogels showed the lowest resistivity ($\sim$1.7 kΩ) and a high storage moduli ($>$10 kPa), demonstrating the multifaceted benefits of graphene nanocomposites. *In situ* polymerization of aniline to give polyaniline−GO composites was aided by the peroxydisulfate counterion of a polymerized ionic liquid, which initiated aniline polymerization along the graphene sheet,[118] giving composites with conductivity of 75 S m^{-1} at 21 wt% GO, five times greater than that of the polyaniline-based composite.

Graphene in bulk heterojunction solar cells

As a versatile electronic material, graphene, CCG and FCCG can function as an electron acceptor, electron donor or additive in bulk heterojunction PV devices depending on the electronics of the chosen counterpart.[119] The π-conjugated framework of graphene and CCG is expected to promote favorable interactions with other conjugated electronic materials such as polythiophene. Zhai and co-workers[120] showed that reduction of GO in a solution with P3HT at elevated temperature, followed by cooling, gave P3HT fibrils emanating from the CCG surface, where the conjugated π-system of graphene served to nucleate P3HT crystallization (Figure 8). Though device performance has not yet been reported for these structures, this simple non covalent grafting from method gives composites with higher conductivity (10^{-3} S m^{-1}) than thin films of the free polymer alone (10^{-4} S m^{-1}).

PV devices have been prepared with active layers of phenyl-functionalized GO to act as the electron carrier blended with poly (3-alkyl thiophenes), followed by thermal annealing that simultaneously converts GO to FCCG and improves poly (3-alkyl thiophene) crystallinity. PCEs as high as 1.4% at 10 wt% FCCG in P3HT or poly-3-octylthiophene were obtained.[121,122] The importance of annealing was established definitively, with PCE improving from 0.15 to 1.1%. Remarkably, the observed open circuit voltage was higher than predicted theoretically, suggesting that the work function of FCCG differs from that of pristine graphene. Scanning electron microscopy characterization of the thin film showed continuous pathways for electron transport at 10 wt% GO in the active layer, and platelet orientation parallel to the underlying substrate (and thus the electrodes) prevented short circuiting.[122,123]

Phenyl-functionalized GO (10 wt%) has also been blended with a P3HT/$PC_{60}BM$ composite (1:1) in attempts to bridge fullerene domains and provide continuous pathways for electron transport. After thermal annealing of devices at 160 °C, to reduce GO to FCCG and generate polymer fibrils, a PCE of 1.4% was obtained, compared with 0.88% PCE without FCCG.[124] FCCG is thought to provide electron transport pathways across fullerene domains, which is supported by a 47% increase in $J_{sc.}$ Covalently connected P3HT−GO was also used in device active layers in attempts to facilitate electronic communication between the two materials.[125] P3HT-functionalized GO prepared by the reaction of hydroxyl-terminated P3HT with acid chloride functionalized GO revealed faster fluorescence decay of the P3HT exciton (380 ps) compared with simple blends of the two materials (476 ps), as determined by time-resolved photoluminescence spectroscopy. Moreover, cyclic voltammetry showed a decrease in the P3HT HOMO level by 0.1 eV, and narrowing of the bandgap by 0.7 eV, upon covalent attachment to GO. An annealed bilayer device of P3HT/2 wt% GO−P3HT and fullerene (C_{60}) gave a PCE of 0.61%, three times greater than the PCE observed for a bilayer of P3HT/GO blend and C_{60}, thereby confirming the importance of the strong electronic interaction provided by covalent connection of the charge carrying components.

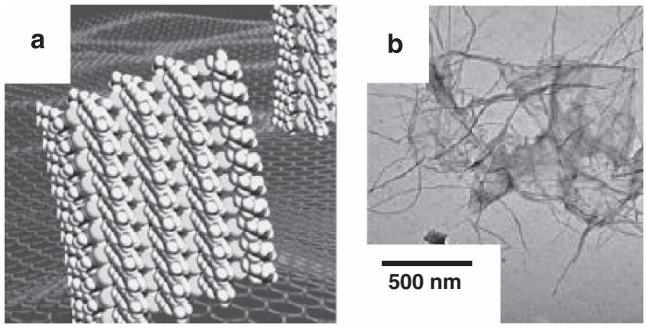

Figure 8 (**a**) Schematic of P3HT nanofibers grown from reduced graphene oxide. (**b**) TEM of P3HT nanofibers with growth nucleated by reduced GO. Reprinted with permission from Chundra *et al.*[120] Copyright 2010 John Wiley and Sons.

OUTLOOK

In summary, combining synthetic advances with processing techniques is giving researchers access to continuous, extended electronically active structures simply by self-assembly in solution, with the resultant properties distinct from the individual molecular components. Although polythiophene fibrils and all carbon-based materials were used to illustrate the concept, there are numerous other materials candidates for such assemblies, including low band gap structures, provided appropriate assembly conditions are found. Synthetic chemistry is crucial for enabling such assemblies, by providing necessary regiochemistry to polymers, and by the integration of functional groups that provide access to processibility, interfacial segregation, cross-linking or hybrid materials formation. As chemists overcome current limitations in the synthesis of well-defined and processable structures, a more diverse range of materials becomes available for integration into devices. Crucial challenges going forward include (1) developing methodology that provides functional handles on these self-assembled systems to enable their precise orientation, such as spanning electrodes in solar cells, (2) ensuring stability of nanoscale phase separation over long time periods, and under challenging thermal and chemical conditions; and (3) improving reproducibility of device fabrication techniques to ensure reliable utilization of the most advanced materials designs. Finally, many of the materials we have described remain at the experimental scale, requiring either scale-up of these specific materials, or translation of the concepts to more easily scalable systems that can be handled easily and manufactured in a cost-effective manner.

ACKNOWLEDGEMENTS

We acknowledge support from the Department of Energy-sponsored PHaSE (Polymers for Harvesting Solar Energy) Energy Frontier Research Center, Grant No. DE-SC0001087.

1 Osaka, I. & McCullough, R. D. Advances in molecular design and synthesis of regioregular polythiophenes. *Acc. Chem. Res.* **41,** 1202–1214 (2008).
2 Sato, M., Tanaka, S. & Kaeriyama, K. Soluble conducting polythiophenes. *J. Chem. Soc. Chem. Commun.* **873** (1986).
3 Chen, T., Wu, X. & Rieke, R. D. Regiocontrolled synthesis of poly(3-alkylthiophenes) mediated by Rieke zinc: their characterization and solid-state properties. *J. Am. Chem. Soc.* **117,** 233–244 (1995).
4 Yokoyama, A., Miyakoshi, R. & Yokozawa, T. Chain-growth polymerization for poly (3-hexylthiophene) with a defined molecular weight and a low polydispersity. *Macromolecules* **37,** 1169–1171 (2004).
5 Miyakoshi, R., Yokoyama, A. & Yokozawa, T. Catalyst-transfer polycondensation. Mechanism of Ni-catalyzed chain-growth polymerization leading to well-defined poly(3-hexylthiophene). *J. Am. Chem. Soc.* **127,** 17542–17547 (2005).
6 Loewe, R. S., Ewbank, P. C., Liu, J., Zhai, L. & McCullough, R. D. Regioregular, head-to-tail coupled poly(3-alkylthiophenes) made easy by the GRIM method: investigation of the reaction and the origin of regioselectivity. *Macromolecules* **34,** 4324–4333 (2001).
7 Loewe, R. S., Khersonsky, S. M. & Mccullough, R. D. A simple method to prepare head-to-tail coupled, regioregular poly(3-alkylthiophenes) using Grignard metathesis. *Adv. Mater.* **11,** 250–253 (1999).
8 Senkovskyy, V., Beryozkina, T., Bocharova, V., Tkachov, R., Komber, H., Lederer, A., Stamm, M., Severin, N., Rabe, J. P. & Kiriy, A. A core-first preparation of poly (3-alkylthiophene) stars. *Macromol. Symp.* **291-292,** 17–25 (2010).
9 Yuan, M., Okamoto, K., Bronstein, H. A. & Luscombe, C. K. Constructing regioregular star poly(3-hexylthiophene) via externally initiated Kumada catalyst-transfer polycondensation. *ACS. Macroletters* **1,** 392–395 (2012).
10 Doubina, N., Jenkins, J. L., Paniagua, S., Mazzio, K., MacDonald, G., Jen, A. K.-Y., Armstrong, N. R., Marder, S. R. & Luscombe, C. K. Surface-initiated synthesis of poly(3-methylthiophene) from indium tin oxide and its electrochemical properties. *Langmuir* **28,** 1900–1908 (2012).
11 Marshall, N., Sontag, S. K. & Locklin, J. Surface-initiated polymerization of conjugated polymer. *Chem. Commun.* **47,** 5681–5689 (2011).
12 Kim, H.-J., Lee, Y. J., Hwang, S. S., Choi, D. H., Yang, H. & Baek, K.-Y. Synthesis of multiarmed poly(3-hexyl thiophene) star polymer with microgel core by GRIM and ATRP methods. *J. Polym. Sci. Part. A: Polym. Chem.* **49,** 4221–4226 (2011).
13 Ihn, K. J., Moulton, J. & Smith, P. Whiskers of poly(3-alkylthiophene)s. *J. Polym. Sci. Part B: Polym. Phys.* **31,** 735–742 (1993).
14 Berson, S., De Bettignies, R., Bailly, S. & Guillerez, S. Poly(3-hexylthiophene) fibers for photovoltaic applications. *Adv. Funct. Mater.* **17,** 1377–1384 (2007).
15 Xin, H., Kim, F. S. & Jenekhe, S. A. Highly efficient solar cells based on poly (3-butylthiophene) nanowires. *J. Am. Chem. Soc.* **130,** 5424–5425 (2008).
16 Niles, E. T., Roehling, J. D., Yamagata, H., Wise, A. J., Spano, F. C., Moule, A. J. & Grey, J. K. J-Aggregate behavior in poly-3-hexylthiophene nanofibers. *The J. of Phys. Chem. Lett.* **3,** 259–263 (2012).
17 Liu, J., Arif, M., Zou, J., Khondaker, S. I. & Zhai, L. Controlling poly(3-hexylthiophene) crystal dimension: nanowhiskers and nanoribbons. *Macromolecules* **42,** 9390–9393 (2009).
18 Yan, H., Yan, Y., Yu, Z. & Wei, Z. Self-assembling branched and hyperbranched nanostructures of poly(3-hexylthiophene) by a solution process. *J. Phys. Chem. C.* **115,** 3257–3262 (2011).
19 Wu, P., Xin, H., Kim, F. S., Ren, G. & Jenekhe, S. A. Regioregular poly (3-pentylthiophene): synthesis, self-assembly of nanowires, high-mobility field-effect transistors, and efficient photovoltaic cells. *Macromolecules* **42,** 8817–8826 (2009).
20 Sirringhaus, H., Brown, P. J., Friend, R. H., Nielson, M. M., Bechgaard, K., Langeveld-Voss, B. M. W., Spiering, A. J. H., Janssen, R. A. J., Meijer, E. W., Herwig, P. & de Leeuw, D. M. Two-dimensional charge transport in conjugated polymers. *Nature* **401,** 685–688 (1999).
21 Bao, Z., Dodabalapur, A. & Lovinger, A. J. Soluble and processable regioregular poly(3-hexylthiophene) for thin film field-effect transistor applications with high mobility. *Appl. Phys. Lett.* **69,** 4108–4110 (1996).
22 Newbloom, G. M., Kim, F. S., Jenekhe, S.a. & Pozzo, D. C. Mesoscale morphology and charge transport in colloidal networks of poly(3-hexylthiophene). *Macromolecules* **44,** 3801–3809 (2011).
23 Moulé, A. J. & Meerholz, K. Controlling morphology in polymer–fullerene mixtures. *Advan. Mater.* **20,** 240–245 (2008).
24 Lee, J. K., Ma, W. L., Braben, C. J., Yuen, J., Moon, J. Y., Lee, K., Bazan, G. G. & Heeger, A. J. Processing additives for improved efficiency from bulk heterojunction solar cells. *J. Am. Chem. Soc.* **130,** 3619–3623 (2008).
25 Samitsu, S., Shimomura, T., Heike, S., Hashizume, T. & Ito, K. Field-effect carrier transport in poly(3-alkylthiophene) nanofiber networks and isolated nanofibers. *Macromolecules* **43,** 7891–7894 (2010).
26 Xin, H., Ren, G., Kim, F. S. & Jenekhe, S. A. Bulk heterojunction solar cells from poly(3-butylthiophene)/fullerene blends: in situ self-assembly of nanowires, morphology, charge transport, and photovoltaic properties. *Chem. Mater.* **20,** 6199–6207 (2008).
27 Ren, G., Wu, P. & Jenekhe, S. A. Solar cells based on block copolymer semiconductor nanowires: effects of nanowire aspect ratio. *ACS Nano* **5,** 376–384 (2011).
28 Li, L., Lu, G. & Yang, X. Improving performance of polymer photovoltaic devices using an annealing-free approach via construction of ordered aggregates in solution. *J. Mater. Chem.* **18,** 1984–1990 (2008).
29 Rice, A. H., Giridharagopal, R., Zheng, S. X., Ohuchi, F. S., Ginger, D. S. & Luscombe, C. K. Controlling vertical morphology within the active layer of organic photovoltaics using poly(3-hexylthiophene) nanowires and phenyl-C61-butyric acid methyl ester. *ACS Nano* **5,** 3132–3140 (2011).
30 Sun, S., Salim, T., Wong, L. H., Foo, Y. L., Boey, F. & Lam, Y. M. A new insight into controlling poly(3-hexylthiophene) nanofiber growth through a mixed-solvent approach for organic photovoltaics applications. *J. Mater. Chem.* **21,** 377–386 (2011).
31 Huynh, W. U., Dittmer, J. J. & Alivisatos, P. Hybrid nanorod-polymer solar cells. *Science* **295,** 2425–2427 (2002).
32 Sun, B. & Greenham, N. C. Improved efficiency of photovoltaics based on CdSe nanorods and poly(3-hexylthiophene) nanofibers. *Phys. Chem. Chem. Phys.* **8,** 3557–3560 (2006).
33 Xu, J., Hu, J., Liu, X., Qiu, X. & Wei, Z. Stepwise self-assembly of P3HT/CdSe hybrid nanowires with enhanced photoconductivity. *Macromol. Rapid Commun.* **30,** 1419–1423 (2009).
34 Ren, S., Chang, L.-Y., Lim, S.-K., Zhao, J., Smith, M., Zhao, N., Bulovic, V., Bawendi, M. & Gradecak, S. Inorganic-organic hybrid solar cell: bridging quantum dots to conjugated polymer nanowires. *Nano. Lett.* **11,** 3998–4002 (2011).
35 Bokel, F. A., Sudeep, P. K., Pentzer, E., Emrick, T. & Hayward, R. C. Assembly of poly(3-hexylthiophene)/CdSe hybrid nanowires by cocrystallization. *Macromolecules* **44,** 1768–1770 (2011).
36 Pentzer, E. B., Bokel, F. a, Hayward, R. C. & Emrick, T. Nanocomposite 'Superhighways' by solution assembly of semiconductor nanostructures with ligand-functionalized conjugated polymers. *Advan. Mater.* **24,** 2254–2258 (2012).
37 Park, S.-J., Kang, S.-G., Fryd, M., Saven, J. G. & Park, S.-J. Highly tunable photoluminescent properties of amphiphilic conjugated block copolymers. *J. Am. Chem. Soc.* **132,** 9931–9933 (2010).
38 Hammer, G., Bokel, F. a., Hayward, R. C. & Emrick, T. Cross-linked conjugated polymer fibrils: robust nanowires from functional polythiophene diblock copolymers. *Chem. Mater.* **23,** 4250–4256 (2011).
39 Lee, E., Hammer, B., Kim, J.-K., Page, Z., Emrick, T. & Hayward, R. C. Hierarchical helical assembly of conjugated poly(3-hexylthiophene)-block-poly(3-triethylene glycol thiophene) diblock copolymers. *J. Am. Chem. Soc.* **133,** 10390–10393 (2011).
40 Wu, J., Pisula, W. & Müllen, K. Graphenes as potential material for electronics. *Chem. Rev.* **107,** 718–747 (2007).
41 Seyler, H., Purushothaman, B., Jones, D. J., Holmes, A. B. & Wong, W. W. H. Hexa-peri-hexabenzocoronene in organic electronics. *Pure Appl. Chem.* **84,** 1047–1067 (2012).
42 Schmidt-Mende, L., Fechtenkotter, A., Mullen, K., Moons, E., Friend, R. H. & MacKenzie, J. D. Self-organized discotic liquid crystals for high-efficiency organic photovoltaics. *Science* **293,** 1119–1122 (2001).
43 Li, J., Kastler, M., Pisula, W., Robertson, J. W. F., Wasserfallen, D., GRimsdale, A. C., Wu, J. & Mullen, K. Organic bulk-heterojunction photovoltaics based on alkyl substituted discotics. *Adv. Funct. Mater.* **17,** 2528–2533 (2007).
44 Schmidtke, J. P., Friend, R. H., Kastler, M. & Mullen, K. Control of morphology in efficient photovoltaic diodes from discotic liquid crystals. *J. Chem. Phys.* **124,** 174704 (2006).
45 Kastler, M., Pisula, W., Wasserfallen, D., Pakula, T. & Mullen, K. Influence of alkyl substituents on the solution- and surface-organization of hexa-peri-hexabenzocoronenes. *J. Am .Chem. Soc.* **127,** 4286–4296 (2005).
46 Fechtenkotter, A., Tchebotareva, N., Watson, M. & Mullen, K. Discotic liquid crystalline hexabenzocoronenes carrying chiral and racemic branched alkyl chains: supramolecular engineering and improved synthetic methods. *Tetrahedron* **57,** 3769–3783 (2001).
47 van de Craats, A. M., Warman, J. M., Fechtenkotter, A., Brand, J. D., Harbison, M. A. & Mullen, K. Record charge carrier mobility in a room-temperature discotic liquid-crystalline derivative of hexabenzocoronene. *Advan. Mater.* **11,** 1469–1472 (1999).
48 Wasserfallen, D., Fischbach, II, Chebotareva, N., Kastler, M., Pisula, W., Jackel, F., Watson, M. D., Schnell, I., Rabe, J. P., Spiess, H. W. & Mullen, K. Influence of hydrogen bonds on the supramolecular order of hexa-peri-hexabenzocoronenes. *Adv. Funct. Mater.* **15,** 1585–1594 (2005).
49 Dou, X., Pisula, W., Wu, J., Bodwell, G. J. & Müllen, K. Reinforced self-assembly of hexa-peri-hexabenzocoronenes by hydrogen bonds: from microscopic aggregates to macroscopic fluorescent organogels. *Chem.—A European J.* **14,** 240–249 (2008).
50 Van De Craats, A. M., Stutzmann, N., Bunk, O., Nielsen, M. M., Watson, M., Mullen, K., Chanzy, H. D., Sirringhaus, H. & Friend, R. H. Meso-epitaxial solution-growth of self-organizing discotic liquid-crystalline semiconductors. *Advan. Mater.* **15,** 495–499 (2003).
51 Pisula, W., Tomovic, Z., El Hamaoui, B., Watson, M. D., Pakula, T. & Mullen, K. Control of the homeotropic order of discotic hexa-peri-hexabenzocoronenes. *Adv. Funct. Mater.* **15,** 893–904 (2005).
52 Samori, P., Yin, X., Tchebotareva, N., Wang, Z., Pakula, T., Jackel, F., Watson, M. D., Venturini, A., Mullen, K. & Rabe, J. P. Self-assembly of electron donor-acceptor dyads into ordered architectures in two and three dimensions: surface patterning and columnar 'double cables'. *J. of the American Chem. Soc.* **126,** 3567–3575 (2004).
53 Wong, W. W. H., Jones, D. J., Yan, C., Watkins, S. E., King, S., Haque, S. A., Wen, X., Ghiggino, K. P. & Holmes, A. B. Synthesis, photophysical, and device properties of novel dendrimers based on a fluorene-hexabenzocoronene (FHBC) core. *Org. Lett.* **11,** 975–978 (2009).
54 Wong, W. W. H., Ma, C.-Q., Pisula, W., Yan, C., Feng, X., Jones, D. J., Mullen, K., Janssen, R. A. J., Bauerle, P. & Holmes, A. B. Self-assembling thiophene dendrimers

with a hexa-peri-hexabenzocoronene core-synthesis, characterization and performance in bulk heterojunction solar cells. *Chem. Mater.* **22,** 457–466 (2010).
55 Hill, J. P., Jin, W., Kosaka, A., Fukushima, T., Ichihara, H., Shimomura, T., Ito, K., Hashizume, T., Ishii, N. & Aida, T. Self-assembled hexa-peri-hexabenzocoronene graphitic nanotube. *Science* **304,** 1481–1483 (2004).
56 Yamamoto, Y., Fukushima, T., Jin, W., Kosaka, A., Hara, T., Nakamura, T., Saeki, A., Seki, S., Tagawa, S. & Aida, T. A glass hook allows fishing of hexa-peri-hexabenzocoronene graphitic nanotubes: fabrication of a macroscopic fiber with anisotropic electrical conduction. *Advan. Mater.* **18,** 1297–1300 (2006).
57 Yamamoto, T., Fukushima, T., Yamamoto, Y., Kosaka, A., Jin, W., Ishii, N. & Aida, T. Stabilization of a kinetically favored nanostructure: surface ROMP of self-assembled conductive nanocoils from a norbornene-appended hexa-peri-hexabenzocoronene. *J. Am. Chem. Soc.* **128,** 14337–14340 (2006).
58 Yamamoto, T., Fukushima, T., Kosaka, A., Jin, W., Yamamoto, Y., Ishii, N. & Aida, T. Conductive one-handed nanocoils by coassembly of hexabenzocoronenes: control of morphology and helical chirality. *Angew. Chemie (International ed. in English)* **47,** 1672–1675 (2008).
59 Yamamoto, Y., Fukushima, T., Saeki, A., Seki, S., Tagawa, S., Ishii, N. & Takuzu, A. Molecular engineering of coaxial donor-acceptor heterojunction by coassembly of two different hexabenzocoronenes: graphitic nanotubes with enhanced photoconducting properties. *J. Am. Chem. Soc.* **129,** 9276–9277 (2007).
60 Yamamoto, Y., Fukushima, T., Suna, Y., Ishii, N., Saeki, A., Seki, S., Tagawa, S., Taniguchi, M., Kawai, T. & Aida, T. Photoconductive coaxial nanotubes of molecularly connected electron donor and acceptor layers. *Science* **314,** 1761–1764 (2006).
61 Wakikawa, Y., Ikoma, T., Yamamoto, Y., Fukushima, T. & Aida, T. Magnetic field effect on the photocarriers in self-assembled hexabenzocoronene nanotubes. *Synthet. Metal* **160,** 275–279 (2010).
62 Saeki, A., Yamamoto, Y., Koizumi, Y., Fukushima, T., Aida, T. & Seki, S. Photoconductivity of self-assembled hexabenzocoronene nanotube: insight into the charge carrier mobilities on local and long-range scales. *The J. of Phys. Chem. Lett.* **2,** 2549–2554 (2011).
63 He, Y., Yamamoto, Y., Jin, W., Fukushima, T., Saeki, A., Seki, S., Ishii, N. & Aida, T. Hexabenzocoronene graphitic nanotube appended with dithienylethene pendants: photochromism for the modulation of photoconductivity. *Advan. Mater.* **22,** 829–832 (2010).
64 Zhang, W., Jin, W., Fukushima, T., Saeki, A., Seki, S. & Aida, T. Supramolecular linear heterojunction composed of graphite-like semiconducting nanotubular segments. *Science* **334,** 340–343 (2011).
65 Kim, Y. H. & Webster, O. W. Water-soluble hyperbrancehd polyphenylene: 'a unimolecular micelle'? *J. Am. Chem. Soc.* **112,** 4592–4593 (1990).
66 Kim, Y. H. & Webster, O. W. Hyperbranched polyphenylenes. *Macromolecules* **25,** 5561–5572 (1992).
67 Simpson, C. D., Mattersteig, G., Martin, K., Gherghel, L., Bauer, R. E., Rader, H. J. & Mullen, K. Nanosized molecular propellers by cyclodehydrogenation of polyphenylene dendrimers. *J. Am. Chem. Soc.* **126,** 3139–3147 (2004).
68 Palermo, V., Morelli, S., Simpson, C., Müllen, K. & Samorì, P. Self-organized nanofibers from a giant nanographene: effect of solvent and deposition method. *J. Mater. Chem.* **16,** 266–271 (2006).
69 Simpson, C. D., Brand, J. D., Berresheim, A. J., Przybilla, L., Rader, J. J. & Mullen, K. Synthesis of a giant 222 carbon graphite sheet. *Chem. Eur. J.* **8,** 1424–1429 (2002).
70 Feng, X., Pisula, W. & Müllen, K. From helical to staggered stacking of zigzag nanographenes. *J. Am. Chem. Soc.* **129,** 14116–14117 (2007).
71 Yang, X., Dou, X., Rouhanipour, A., Zhi, L., Rader, H. J. & Mullen, K. Two-dimensional graphene nanoribbons. *.J Am. Chem. Soc.* **130,** 4216–4217 (2008).
72 Luo, J., Cote, L. J., Tung, V. C., Tan, A. T. L., Goins, P. E., Wu, J. & Huang, J. Graphene oxide nanocolloids. *J. Am. Chem. Soc.* **132,** 17667–17669 (2010).
73 Peng, J., Gao, W., Gupta, B. K., Liu, Z., Romero-Arburto, R., Ge, L., Song, L., Alemany, L. B., Zhan, X., Gao, G., Vithayathil, S. A., Kaipparettu, B. A., Marti, A., Hayashi, T., Zhu, J.-J. & Ajayan, P. M. Graphene quantum dots derived from carbon fibers. *Nano. Lett.* **12,** 844–849 (2012).
74 Novoselov, K. S., Geim, A. K., Morozov, S. V., Jiang, D., Zhang, Y., Dubonos, S. V., Grigorieva, I. V. & Firsov, A. A. Electric field effect in atomically thin carbon films. *Science* **306,** 666–669 (2004).
75 Lee, C., Wei, X., Kysar, J. W. & Hone, J. Measurement of the elastic properties and intrinsic strength of monolayer graphene. *Science* **321,** 385–388 (2008).
76 Kato, M. & Usuki, A. *Polymer-clay nanocomposites* 97–109 (John Wiley & Sons Ltd., West Sussex, England, 2000).
77 Geim, A. K. & Novoselov, K. S. The rise of graphene. *Nat. Mater.* **6,** 183–191 (2007).
78 Zhang, Y., Tan, Y.-W., Stormer, H. L. & Kim, P. Experimental observation of the quantum Hall effect and Berry's phase in graphene. *Nature* **438,** 201–204 (2005).
79 Tassin, P., Koschny, T., Kafesaki, M. & Soukoulis, C. M. A comparison of graphene, superconductors and metals as conductors for metamaterials and plasmonics. *Nat. Photonics.* **6,** 259–264 (2012).
80 Xu, Z., Tai, G., Zhou, Y., Gao, F. & Wong, K. H. Self-charged graphene battery harvests electricity. *arXiv:1203.0161.*
81 Ji, H., Zhang, L., Pettes, M. T., Li, H., Chen, S., Shi, L., Piner, R. & Ruoff, R. S. Ultrathin graphite foam: a three-dimensional conductive network for battery electrodes. *Nano Lett.* **12,** 2446–2451 (2012).
82 Shahil, K. M. F. & Balandin, A. A. Graphene-multilayer graphene nanocomposites as highly efficient thermal interface materials. *Nano Lett* **12,** 861–867 (2012).
83 Konstantatos, G., Badioli, M., Gaudreau, L., Osmond, J., Bernechea, M., de Arquer, F. P. G., Gatti, F. & Koppens, F. H. L. Hybrid graphene-quantum dot phototransistors with ultrahigh gain. *Nature Nanotechnology* **7,** 363–368 (2012).
84 Torrisi, F., Hasan, T., Wu, W., Sun, Z., Lombardo, A., Kulmala, T. S., Hsieh, G.-W., Jung, S., Bonaccorso, F., Paul, P. J., Chu, D. & Ferrari, A. C. Inkjet-printed graphene electronics. *ACS Nano* **6,** 2992–3006 (2012).
85 Bae, S., Kim, G., Lee, Y., Xu, X., Park, J.-S. & Zheng, Y. Roll-to-roll production of 30-inch graphene films for transparent electrodes. *Nature Nanotechnology* **5,** 574–578 (2010).
86 Vogt, P., De Padova, P., Quaresima, C., Avila, J., Frantzeskakis, E., Asensio, M., Resta, A., Ealet, B. & Le Lay, G. Silicene: compelling experimental evidence for graphenelike two-dimensional silicon. *Phys. Rev. Lett.* **108,** 1–5 (2012).
87 Malko, D., Neiss, C., Viñes, F. & Görling, A. Competition for graphene: graphynes with direction-dependent Dirac cones. *Phys Rev Lett* **108,** 086804 (2012).
88 Lee, W. H., Suk, J. W., Chou, H., Lee, J., Hao, Y., Wu, Y., Piner, R., Akinwande, D., Kim, K. S. & Ruoff, R. S. Selective-area fluorination of graphene with fluoropolymer and laser irradiation. *Nano Lett.* **12,** 2374–2378 (2012).
89 Nair, R. R., Ren, W., Jalil, R., Riaz, I., Kravets, V. G., Britnell, L., Blake, P., Schedin, F., Mayorov, A. S., Yuan, S., Katsnelson, M. I., Chen, H.-M., Strupinski, W., Bulusheva, L. G., Okotrub, A. V., Grigorieva, I. V., Grigorenko, A. N., Novoselov, K. S. & Geim, A. K. Fluorographene: a two-dimensional counterpart of Teflon. *Small* **6,** 2877–2884 (2010).
90 Hummers, W. S. & Offeman, R. E. Preparation of graphitic oxide. *J. Am. Chem. Soc.* **80,** 1339 (1958).
91 Hu, H., Wang, x., Wang, J., Wan, L., Liu, F., Zheng, H., Chen, R. & Xu, C. Preparation and properties of graphene nanosheets–polystyrene nanocomposites via *in situ* emulsion polymerization. *Chem. Phys. Lett.* **484,** 247–253 (2010).
92 Salavagione, H. J., Martínez, G. & Ellis, G. Recent advances in the covalent modification of graphene with polymers. *Macromol. Rapid Commun.* **32,** 1771–1789 (2011).
93 Pei, S. & Cheng, H.-M. The reduction of graphene oxide. *Carbon N. Y.* **50,** 3210–3228 (2012).
94 Choi, E.-K., Jeon, I.-Y., Oh, S.-J. & Baek, J.-B. 'Direct' grafting of linear macromolecular 'wedges' to the edge of pristine graphite to prepare edge-functionalized graphene-based polymer composites. *J Mater Chem* **20,** 10936–10942 (2010).
95 Cote, L. J., Cruz-Silva, R. & Huang, J. Flash reduction and patterning of graphite oxide and its polymer composite. *J. Am. Chem. Soc.* **131,** 11027–11032 (2009).
96 Si, Y. & Samulski, E. T. Synthesis of water soluble graphene. *Nano Lett.* **8,** 1679–1682 (2008).
97 Stankovich, S., Piner, R., Nguyen, S. & Ruoff, R. Synthesis and exfoliation of isocyanate-treated graphene oxide nanoplatelets. *Carbon N. Y.* **44,** 3342–3347 (2006).
98 Kuila, T., Bose, S., Hong, C. E., Uddin, M. E., Khanra, P., Kim, N. H. & Lee, J. H. Preparation of functionalized graphene/linear low density polyethylene composites by a solution mixing method. *Carbon N. Y.* **49,** 1033–1037 (2011).
99 Pham, V. H., Cuong, T. V., Dang, T. T., Hur, S. H., Kong, B.-S., Kim, E. J., Shin, E. W. & Chung, J. S. Superior conductive polystyrene–chemically converted graphene nanocomposite. *J. Mater. Chem.* **21,** 11312–11316 (2011).
100 Wei, T., Luo, G., Fan, Z., Zheng, C., Yan, J., Yao, C., Li, W. & Zhang, C. Preparation of graphene nanosheet/polymer composites using *in situ* reduction–extractive dispersion. *Carbon N Y* **47,** 2296–2299 (2009).
101 Pang, H., Zhang, Y.-C., Chen, T., Zeng, B.-Q. & Li, Z.-M. Tunable positive temperature coefficient of resistivity in an electrically conducting polymer/graphene composite. *Appl. Phys. Lett.* **96,** 251907 (2010).
102 Tung, V. C., Huang, J.-H., Tevis, I., Kim, F., Kim, J., Chu, C.-W., Stupp, S. I. & Huang, J. Surfactant-free water-processable photoconductive all-carbon composite. *J. Am. Chem. Soc.* **133,** 4940–4947 (2011).
103 Kim, F., Cote, L. J. & Huang, J. Graphene oxide: surface activity and two-dimensional assembly. *Advan. Mater.* **22,** 1954–1958 (2010).
104 Kim, J., Cote, L. J., Kim, F., Yuan, W., Shull, K. R. & Huang, J. Graphene oxide sheets at interfaces. *J. Am. Chem. Soc.* **132,** 8180–8186 (2010).
105 Cote, L. J., Kim, J. & Huang, J. Langmuir-Blodgett assembly of soft carbon sheets. *Mater. Res. Soc. Symp. Proc.* **1344,** 3–9 (2011).
106 Gao, Y., Chen, X., Xu, H., Zou, Y., Gu, R., Xu, M., Jen, A. K. & Chen, H. Highly-efficient fabrication of nanoscrolls from functionalized graphene oxide by Langmuir-Blodgett method. *Carbon N. Y.* **48,** 4475–4482 (2010).
107 Zheng, Q., Ip, W. H., Lin, X., Yousefi, N., Yeung, K. K., Li, Z. & Kim, J.-K. Transparent conductive films consisting of ultralarge graphene sheets produced by Langmuir-Blodgett assembly. *ACS Nano* **5,** 6039–6051 (2011).
108 Cooper, A. I. Nanoporous organics enter the cage age. *Angew. Chemie (International Ed. in English)* **50,** 996–998 (2011).
109 Colson, J. W., Woll, A. R., Mukherjee, A., Levendorf, M. P., Spitler, E. L., Shields, V. B., Spencer, M. G., Park, J. & Dichtel, W. R. Oriented 2D covalent organic framework thin films on single-layer graphene. *Science* **332,** 228–231 (2011).
110 Spitler, E. L., Koo, B. T., Novotney, J. L., Colson, J. W., Uribe-Romo, F. J., Gutierrez, G. D., Clancy, P. & Dichtel, W. R. A 2D covalent organic framework with 4.7-nm pores and insight into its interlayer stacking. *J. Am. Chem. Soc.* **133,** 19416–19421 (2011).
111 Mann, J. a, Rodríguez-López, J., Abruña, H. D. & Dichtel, W. R. Multivalent binding motifs for the noncovalent functionalization of graphene. *J. Am. Chem. Soc.* **133,** 17614–17617 (2011).

112 Qi, X., Pu, K.-Y., Li, H., Zhou, X., Wu, S., Fan, Q.-L., Liu, B., Boey, F., Huang, W. & Zhang, H. Amphiphilic graphene composites. *Angew. Chemie (International ed. in English)* **49,** 9426–9429 (2010).
113 Yang, H., Zhang, Q., Shan, C., Li, F., Han, D. & Niu, L. Stable, conductive supramolecular composite of graphene sheets with conjugated polyelectrolyte. *Langmuir* **26,** 6708–6712 (2010).
114 Ramuz, M. P., Vosgueritchian, M., Wei, P., Wang, C., Gao, Y., Wu, Y., Chen, Y. & Bao, Z. Evaluation of solution-processable carbon-based electrodes for all-carbon solar cells. *ACS Nano* **6,** 10384–10395 (2012).
115 Su, Q., Pang, S., Alijani, V., Li, C., Feng, X. & Mullen, K. Composites of graphene with large aromatic molecules. *Advan. Mater.* **21,** 3191–3195 (2009).
116 Luo, Y.-B., Cheng, J.-S., Ma, Q., Feng, Y.-Q. & Li, J.-H. Graphene-polymer composite: extraction of polycyclic aromatic hydrocarbons from water samples by stir rod sorptive extraction. *Anal. Methods* **3,** 92–98 (2011).
117 Bai, H., Sheng, K., Zhang, P., Li, C. & Shi, G. Graphene oxide/conducting polymer composite hydrogels. *J. Mater. Chem.* **21,** 18653–18658 (2011).
118 Zhou, X., Wu, T., Hu, B., Yang, G. & Han, B. Synthesis of graphene/polyaniline composite nanosheets mediated by polymerized ionic liquid. *Chem. Commun.* **46,** 3663–3665 (2010).
119 Guldi, D. M. & Sgobba, V. Carbon nanostructures for solar energy conversion schemes. *Chem. Commun.* **47,** 606–610 (2011).
120 Chunder, A., Liu, J. & Zhai, L. Reduced graphene oxide/poly(3-hexylthiophene) supramolecular composites. *Macromol. Rapid Commun.* **31,** 380–384 (2010).
121 Liu, Z., Liu, Q., Huang, Y., Ma, Y., Yin, S., Zhang, X., Sun, W. & Chen, Y. Organic photovoltaic devices based on a novel acceptor material: graphene. *Advan. Mater.* **20,** 3924–3930 (2008).
122 Liu, Q., Liu, Z., Zhang, X., Yang, L., Zhang, N., Pan, G., Yin, S., Chen, Y. & Wei, J. Polymer photovoltaic cells based on solution-processable graphene and P3HT. *Adv Funct Mater* **19,** 894–904 (2009).
123 Liu, Q., Liu, Z., Zhang, X., Zhang, N., Yang, L., Yin, S. & Chen, Y. Organic photovoltaic cells based on an acceptor of soluble graphene. *Appl. Phys. Lett.* **92,** 223303 (2008).
124 Liu, Z., He, D., Wang, Y., Wu, H. & Want, J. Graphene doping of P3HT:PCBM photovoltaic devices. *Synthet. Metal.* **160,** 1036–1039 (2010).
125 Yu, D., Yang, Y., Durstock, M., Baek, J. & Dai, L. Soluble P3HT-grafted graphene for efficient bilayer heterojunction photovoltaic devices. *ACS Nano* **4,** 5633–5640 (2010).

Todd Emrick is Professor of Polymer Science and Engineering at the University of Massachusetts Amherst, and is Director of the National Science Foundation supported Materials Research Science and Engineering Center on Polymers at the University of Massachusetts. He completed his PhD with Professor Philip Eaton at the University of Chicago in 1997, where he synthesized rigid-rod oligomers from the strained hydrocarbon cubane. He then worked as a postdoctoral associate with Professor Jean Fréchet at the University of California Berkeley, preparing dendritic-linear block copolymers and functional hyperbranched polymers and adhesives. He has been on the faculty at the University of Massachusetts Amherst since 2001, with active research projects in the areas of novel monomer and polymer synthesis, polymer-nanoparticle composites, hybrid materials containing quantum dots, surfactants in solution and at interfaces, self-healing concepts and polymer-based approaches to cancer therapeutics and gene therapy.

Emily Pentzer, a native of Bedford, Indiana, received a Bachelors of Science in chemistry with highest honors from Butler University in 2001 and a PhD in organic chemistry from Northwestern University in 2010, where she was a National Science Foundation graduate research fellow. Her thesis work focused on using ring closing metathesis to prepare unsaturated 7- and 8-membered lactones and lactams, which could in turn be used as monomers in ring opening metathesis polymerization to yield biodegradable polymers under mild reaction conditions. Emily joined the group of Todd Emrick in the Polymer Science and Engineering Department at the University of Massachusetts Amherst as a postdoctoral associate in the summer of 2010. Her current work, supported by the Department of Energy-funded Polymers for Harvesting Solar Energy Energy Frontier Research Center, focuses on the synthesis and assembly of functionalized electronically active materials, which serve as templates for higher order *p*-type/*n*-type assemblies.